A MULTISPECTRAL REMOTE SENSING INVESTIGATION OF LEAF AREA INDEX AT BLACK ROCK FOREST, NY

A thesis presented to

the faculty of

the College of Arts and Sciences of Ohio University

In partial fulfillment

of the requirements for the degree

Master of Arts

David Z. May

November 2006

This thesis entitled

A MULTISPECTRAL REMOTE SENSING INVESTIGATION OF LEAF AREA INDEX AT BLACK ROCK FOREST, NY

by

DAVID Z. MAY

has been approved for

the Department of Geography

and the College of Arts and Sciences by

James Kurt Lein

Professor of Geography

Benjamin M. Ogles

Dean, College of Arts and Sciences

Abstract

MAY, DAVID Z., M.A., November 2006. Geography

A MULTISPECTRAL REMOTE SENSING INVESTIGATION OF LEAF AREA INDEX AT BLACK ROCK FOREST, NY (71 pp.)

Director of Thesis: James Kurt Lein

A remote sensing investigation was conducted in June 2000 in a mixed-oak forest undergoing successional changes at Black Rock Forest, NY. Leaf litter data was collected throughout the fall of 2000 to assess productivity at the site and to obtain species-specific leaf area (LAI_{SPP}) data for *Acer rubrum*, *Quercus prinus*, and *Quercus rubrum*. There were two objectives in this investigation: to determine (1) whether spectral differences exist at branch-level between the oak and maple groups at this site, and (2) whether the remotely-sensed canopy-level classifications are able to produce estimates of canopy cover for red maple that reflect the forest composition identified with the LAI_{SPP} information. Significant multispectral differences were identified for all groups at the branch-level. Canopy-level analyses were restricted to the 550 nm wavelength because of calibration issues with the imaging system. These images were processed using soft classification methods, and produced canopy cover maps of questionable accuracy.

Approved:

James Kurt Lein

Professor of Geography

Acknowledgements

I would like to thank my committee: James K. Lein, Dorothy Sack, Ronald H. Isaac, Christopher G. Boone, and Kim J. Brown. Data collection for this project was made possible through grant funding provided by the Black Rock Forest Consortium (http://www.blackrockforest.org/). This project was facilitated by William Schuster, Kevin Griffin, and the Lamont-Doherty Earth Observatory. Special thanks to Bill Richards at NY Film Flyers (http://www.nyfilmflyers.com/) and Milton Smith from the University of Washington for the use of the digital imaging system used in this investigation. I would like to thank Kim J. Brown and Stephanie A. Bohlman, for collecting and assisting in the processing of all data used in this study. Thanks to Gail Yamada from the University of Washington Remote Sensing Group for obtaining spectrometer values of the calibration panels. Finally, I would like to thank the faculty, staff, and students at the Ohio University Department of Geography for their assistance and support throughout this project.

Table of Contents

Abstract 3

Acknowledgements 4

List of Tables 6

List of Figures 7

Chapter 1: Introduction 8

Chapter 2: Literature Review 12
Leaf-Level Spectral Properties 12
Branch-Level Spectral Properties 13
LAI Estimation from Leaf Litter Collection 14
Remote Sensing and LAI 15
Remote Sensing Approaches for Mapping at the Species-Level 17
Remote Sensing Considerations in the Eastern Deciduous Forest 18
Image Classification 20
Dempster-Shafer Theory of Evidence 23

Chapter 3: Site Description 26

Chapter 4: Materials & Methods 27
Leaf Litter/Leaf Area Measurements 27
Image Acquisition 28
Branch-Level Spectral Analyses 29
Canopy-Level Spectral Analyses 30

Chapter 5: Results & Discussion 34
Branch-Level Spectral Analyses 34
LAI_{SPP} Measurements at Black Rock Forest 35
Canopy-Level Spectral Analyses 36
Comparisons of Image Classification Results With LAI 39

Chapter 6: Conclusion 41

References 63

List of Tables

Table Page

1: Basal area and stem density at Black Rock Forest 44
2: Combinations of classes in the Dempster-Shafer Theory of Evidence Decision Frame 45
3: 2000 LAI_{SPP} leaf litter trap data from the Cascade Brook Watershed of Black Rock Forest 46
4: Mean branch-level spectra from one-way ANOVA analyses 47

List of Figures

Figures Page

1.0 Topographic map of the Black Rock Forest 48
1.1 Zoom scale topographic map of the study areas at Black Rock Forest 49

4.0 Methods flowchart of leaf litter collection and LAI_{SPP} calculation 50
4.1 Methods flowchart of branch-level spectral analyses.....51
4.2 Branch-level images from the cherry picker of *A. rubrum*, *Q. prinus*, and *Q. rubra*.....52
4.3 Methods flowchart of canopy-level data acquisition and image processing 53
4.4 Mosaicked green band imagery (550 nm) of the study area.....54
4.5 False color image demonstrating feature class collection of training data used in image classification.....55
4.6 BELCLASS belief classified surface of [Maple].....56
4.7 BELCLASS belief classified surface of [Other].....57
4.8 BELCLASS belief classified surface of [Shadow].....58
4.9 BELCLASS belief classified surface of ignorance expressed as classification uncertainty.....59
4.10 Approach 1 results from MAXSET 60
4.11 Approach 2 results from MAXSET 61
4.12 Approach 3 results from MAXSET 62

Chapter 1

Introduction

Temperate mixed-oak-dominated (*Quercus* sp.) forests in the Northeastern United States are currently undergoing measurable changes in species composition and successional patterns. Many factors are contributing to the decline of mixed oak dominated forests, including: land-use change patterns, fire suppression, gypsy moth predation, climate change, seed predation, poor germination strategies, poor recruitment of oak saplings in the understory, and the inability to compete with more shade-tolerant species (Abrams 1998, Lorimer 1984, Tift and Fajvan 1999). The most striking change to the species composition in the Eastern Deciduous Forest is the encroaching presence and dominance of red maple (*Acer rubrum* L.). This shift has been termed, "The Red Maple Paradox" (Abrams 1998).

Red maple is a supergeneralist species, meaning that it grows well along a broad range of conditions, versus being specialized for growth in a specific ecological niche. Historically, the red maple was restricted to mesic sites, but due to fire suppression it has been able to expand into areas previously dominated by mixed-oak forests exhibiting limiting amounts of soil moisture, soil nutrients, and light availability. Multitudinous factors have given the red maple a distinct advantage over co-occurring oak species, including its early phenological leaf-out, early spring germination, high fecundity, development of short-term seed banks, ability to survive in the understory under suppressed light environments, and its rapid exploitation of gaps in the canopy following disturbance events. Implications of global warming and climate change are also factors

that may be contributing to the dramatic range into which the red maple is expanding. Since mixed-oak-dominated forests, where red maple is increasing in dominance, are positioned along the hypothetical expansion zone, it is anticipated that they will expand across the current range occupied by Northeastern mixed forests.

The best way to evaluate the changes occurring in forest ecosystems is through the measurement of both the productivity (biomass accumulation) and the contribution of individual species over time. There are a number of forest mensuration methods that can be used to monitor changes in forest ecosystems. One of the most valuable and robust forest metrics is the measurement of forest leaf area, measured by leaf area index (LAI). LAI is a dimensionless, structural metric that was first used to measure field crops (Watson 1947), and is defined as the amount of leaf area (m^2) in a canopy per unit of ground area (m^2). Forest leaf area is one of the critical factors that limit net productivity in a system, because leaves function as the surface area for gas and energy exchange. Species-specific leaf area measurements (LAI_{SPP}) represent valuable information, as different species and functional groups (e.g. pioneer, shade-tolerant, etc.) have large differences in their rates of growth and biogeochemical properties (Smith *et al.* 1997). The robustness of LAI_{SPP} measurements is unique in that these data represent a higher value informational source over other forest metrics (e.g. basal area, stem density, etc.), because they can be used to drive primary productivity models from the scale of an individual tree to the biome level.

Many methods exist to measure the leaf area of a system, ranging from direct measurement techniques (litter baskets and destructive harvest) to indirect remotely-sensed techniques (Fassnacht *et al.* 1994, Gower *et al.* 1999, Jurik *et al.* 1985, Neumann

et al. 1989, Weiss *et al.* 2004). The direct measurement of LAI is costly in time, labor, and finance. These constraints have led researchers to evaluate the utility of remotely-sensed methods, capable of providing large data sets at a fraction of the cost. Remote sensing of forested ecosystems represents an attractive tool for researchers in that it can provide repeatable observations obtained at the canopy-level. This provides a critical new vantage point for conducting forest research; traditionally, observations have been confined to the forest floor.

There are two objectives in this investigation at Black Rock Forest, NY (BRF): to determine (1) whether spectral differences exist at branch-level between the oak and maple groups at this site, and (2) whether the remotely-sensed canopy-level classifications are able to produce estimates of canopy cover for red maple that reflect the forest composition identified with the LAI_{SPP} information. (Figure 1.0, 1.1). LAI_{SPP} information was derived from species partitioned leaf litter trap measurements obtained throughout the fall of 2000. Aerial and branch-level remotely-sensed data were collected with an experimental camera system in a helicopter and a cherry picker in late June, 2000. Branch-level imagery was used to determine whether spectral differences exist between the three dominant tree species at the site [*Acer rubrum* L. (red maple), *Quercus prinus* L. syn. *Quercus montana* Willd. (chestnut oak), and *Quercus rubra* L. (red oak)]. Canopy-level imagery was then used to create maple classes of canopy cover, using spectral training data on species of known identity and a soft classifier based on the Dempster-Shafer Theory of Evidence algorithm. The quantitative class membership data of maple proportions observed with the classified aerial imagery were then compared with the LAI_{SPP} information.

Previous investigations at BRF provide evidence, from basal area and stem density data, that contradicts species assemblages and species productivity levels at this site (Turnbull *et al.* 2002) (Table 1). The potential application of this work is significant, since mixed-oak forests cover a large area in the United States and the BRF site is at the northern limit of oak distribution. There is also a large body of long-term ecological research at this site (Lorimer 1984, Turnbull *et al.* 2002, Tyron 1930), and at nearby hardwood forests including the Harvard Forest (Motzkin *et al.* 1999, Waring and Schlesinger 1995, Williams *et al.* 1996) and the Hubbard Brook Environmental Forest (Bormann *et al.* 1970, Leckie *et al.* 1998, Likens 1999, Whittaker *et al.* 1974). The ability to detect species groups (oak and maple) in mixed-oak forests with remotely-sensed techniques may provide a rapid method for researchers to enhance the understanding of successional dynamics and biomass accumulation in these forest ecosystems. The LAI_{SPP} information presented in this thesis will serve as a valuable contribution to other researchers, since it presents a baseline measurement of forest productivity at this site and can serve as a validation test site for future remote sensing projects and modeling efforts.

Chapter 2

Literature Review

Leaf-Level Spectral Properties

The optical properties of leaves have many factors that influence how electromagnetic radiation (EMR) will interact with plant structures. These factors include radiation regime, pigment content and concentration, dry matter per leaf unit area, internal structure, leaf surface structures, and leaf thickness (Ross 1981). The amount of EMR that is reflected, transmitted, or absorbed by leaves ultimately depends upon the energy level and resulting wavelength of incoming EMR.

Vegetation properties in the visible (VIS) region of the spectrum (400-700 nm) are characterized by low reflectance and transmittance, and strong absorption of light by plant pigments. The abundance of chlorophyll dominates the spectral response in the VIS, as there is 5-10 times more chlorophyll than carotenoid pigments present in vegetation (Belward 1991). Green vegetation exhibits absorption in the violet-blue or red wavelengths (420, 490, 660 nm); thus, a reflectance peak at 550 nm (green) gives vegetation its distinct appearance. At the end of the growing season, senescence of vegetation occurs, where the chlorophylls degrade faster than the carotenes (Sanger 1971). This yields an increase in red reflectance, which has been applied in differential species classification (Ramsey III *et al.* 2005a, Ramsey III *et al.* 2005b). Near-infrared (NIR) EMR is not absorbed by plant pigments, because it lacks the necessary energy to drive photochemical reactions. The dominant factor that controls the spectral properties of vegetation in the NIR is the internal structure of leaves from photon scattering at the

air-cell interfaces within the leaf spongy mesophyll (Boyer *et al.* 1988, Gates *et al.* 1965, Sinclair *et al.* 1971, Woolley 1971).

Leaf spectral properties vary widely based on the external structures on the surface, such as trichomes and waxes (Gausman 1985, Jacquemoud *et al.* 1995, Reicosky 1994, Slaton *et al.* 2001). Seasonal changes and leaf age also contribute to the variability in spectral reflectance (Blackburn and Milton1995, Brakke *et al.* 1993, Roberts *et al.* 1998). The presentation of the leaves (erectophilic, planophilic), position in the canopy (Howard 1991, Jacquemoud *et al.* 1995), and the angle of solar incidence (Brakke *et al.* 1993) are all considerable factors. Nutrient availability may also play a role in characterizing spectral properties (Martin and Aber1997, McLellan *et al.* 1991). A number of factors contribute to the spectral variability often present in complex remotely-sensed scenes, making the spectral separation of different vegetation types and species difficult (Cochrane 2000, Price 1992, Price 1994).

Branch-Level Spectral Properties

The NIR reflectance of canopies exhibits a higher reflectance than that of individual leaves. The majority of NIR EMR is transmitted through individual leaves, although a fraction of this transmitted light is then scattered by subsequent leaf layers. This additive effect of multiple leaf layers in the NIR reflectance has been observed in past research (Hoffer 1978, Thomas *et al.* 1967). When adding extra layers of leaves does not produce an increase in the NIR reflectance, an asymptotic relationship known as the near-infrared infinite reflectance is reached (Belward 1991). This relationship between increased reflectance as the number of leaf layers increases is fundamentally linked to LAI.

Canopy reflectance is driven by differences in plant structure. Plants differ in how they arrange leaves and stems in three-dimensional space. These leaves and stems act as "scatterers," where photons interact with multiple surfaces, including other leaves, non-photosynthetic vegetation (NPV= woody stems, shoots, etc.), litter, background soils, and other encompassed scene elements. Photon interactions with vegetation in vertical space is highly non-linear (Asner *et al.* 1997, Borel and Gerstl 1994, Myneni *et al.* 1989, Ross 1981), whereas the horizontal mixing of vegetation across the landscape is a linear process (Roberts *et al.* 1993). These factors complicate the remote sensing of vegetation, which essentially samples the optical depth of a forest canopy. Factors like LAI and leaf angle distribution (LAD) act as the dominant controls on canopy reflectance, with the exception of sparse canopy cover and variable soil reflectance (Asner 1998). Previous investigations have demonstrated that vegetation reflectance decreases as the path length of the observations increases, and when scene complexity expands to include other spectral surfaces (Williams 1991).

LAI Estimation from Leaf Litter Collection

LAI can be determined through the calculation of specific leaf area (SLA). SLA is determined by establishing a relationship between the area and dry weight of leaves collected in leaf litter traps throughout a growing season. Leaves are collected in standardized leaf litter traps (having the same surface area), and it is assumed that the litter collected represents the average leaf fall within a stand. A representative sample of leaves is rehydrated and the leaf area is measured with a leaf area meter. Leaf litterfall collection and the derivation of SLA is the most reliable method to calculate LAI, and serves as the standard when comparing estimation techniques (Chason *et al.* 1991,

Fassnacht *et al.* 1997, Liu *et al.* 1997). The development of new remotely-sensed methodologies to measure LAI is constantly being pursued, as "*in situ"* leaf litterfall collection and measurement is a costly and laborious process. Changes in both LAI and vegetation cover of less than 10% are difficult to verify through field and remote sensing measurements, because the error associated with field measurements is typically ≥ 10% (Asner 1998).

Remote Sensing and LAI

Leaves in plant canopies act as the primary surface of energy exchange within terrestrial ecosystems, and represent the optical depth of a canopy. The LAI metric has been highly correlated with a number of ecosystem processes, including canopy light interception (Fassnacht *et al.* 1994, Nemani *et al.* 1993), site water balance (Grier and Running 1977), above-ground net primary production (Gholz 1982), and total net primary production (Gower *et al.* 1992). The dimensionless aspect of LAI allows for its use in modeling efforts across spatial scales ranging from landscapes to individual crowns. These correlations with LAI have led to the development of large modeling efforts that use LAI as an input for biogeochemical, physiological, hydrological, climatological, and general circulation models (Bonan 1998, Jin and Zhang 2002; Kergoat 1998, Sellers *et al.* 1997). Satellite remote sensing provides the most effective method to collect global data on a regular basis without being in direct contact with the features being studied. Aerial remote sensing investigations are ideally suited for local surveys, due to their high signal-to-noise ratio and their high degree of flexibility for data acquisition.

A number of remote sensing investigations have estimated LAI through the use of vegetation indices (VI), or canopy radiation models. Canopy radiation models are computationally costly equations that model photon interactions. By contrast, VI are relatively easy to compute and interpret. VI are simple algorithms that emphasize vegetation by differencing the spectral response of two or more spectral wavelengths. LAI is estimated from VI based on empirical regression-based relationships. The theory underlying these relationships is that increases in LAI trigger a decrease in red reflectance due to absorption by plant pigments, with NIR reflectance increasing because of scattering events (Knipling 1970). VI and canopy radiation models were originally developed to estimate the productivity of agricultural crops in structurally simplistic and predictable canopies. The logic supporting the use of VI is that as more leaf layers are present within a plant canopy there will be an increase in chlorophyll abundance leading to increases in energy absorption (Myneni *et al.* 1995). The development of VI began with the Ratio-Based Index (RVI), which uses a ratio of NIR and red EMR (RVI = NIR / red) (Jordan 1969). This led to the concept (Kriegler *et al.* 1969) and implementation (Rouse *et al.* 1974) of the Normalized Difference Vegetation Index (NDVI). The NDVI uses different wavelengths of red and NIR EMR [NDVI = (NIR - red) / (NIR + red)], and serves as the most well-documented VI used in remote sensing analyses for the estimation of LAI.

The ability to predict LAI values greater than 3.0 with the NDVI becomes hampered due to a saturation in canopy reflectance and the non-linear relationship between LAI and the NDVI (Baret and Guyot 1991). This is important because forests with LAI values greater than 3.0 comprise one-third of the terrestrial land surface

(Waring and Schlesinger 1985). Deciduous forests typically have LAI values ranging from 5.0-8.0 (Larcher 1995), making accurate remote sensing assessments of LAI using the NDVI in these ecosystems impossible. Many remote sensing studies estimate LAI at coarse scales at the level of land cover (e.g., grassland, forest, etc.). These estimates fail to account for the inherent variability in productivity between different species across the landscape. Species-specific estimates of LAI (LAI_{SPP}) can provide valuable information regarding the contribution of individual species to the total productivity of forest ecosystems.

Remote Sensing Approaches for Mapping at the Species-Level

The identification of individual species and functional groups have prompted many researchers to employ remote sensing techniques to identify, classify, and map specific vegetation types. Invasive species that have distinct spectral properties have been mapped (Glenn *et al.* 2005, Ramsey III *et al.* 2005a, Ramsey III et al. 2005b). Other workers have relied on the spectral properties of individual species (Key *et al.* 2001, Leckie *et al.* 1992, Rohde and Olson 1972, van Aardt and Wynne 2001, Warner *et al.* 2000). The ability to isolate rare, endangered, or threatened plant species with remote sensing technologies is also critical to effective management of forest resources (Brandtberg 2003).

Landscape scale classifications on different species assemblages can be made on the basis of leaf-level and branch-level spectral properties (Asner *et al.* 2000, Cochrane 2000, Roberts *et al.* 1993). Conducting spectral classifications over large geographic areas requires the use of extensive field- and lab-based reflectance data to measure the differences in spectral and chemical properties as a basis for separation at the species-

level (Asner 1998, Martin *et al.* 1998, Ramsey III *et al.* 2005a). This approach has been widely used throughout hyperspectral studies, but has not been readily employed with the same frequency in multispectral investigations. Many multispectral sensors are incapable of fully exploiting these data, since they convolve broad regions of the spectrum and lack the necessary spectral resolution. The most important aspect of this field- and lab-based approach is that it provides a reflectance continuum of discrete wavelength samples (~10 nm) that detail subtle changes in reflectance across a wide range of the spectrum. The ability to use laboratory analyses to determine the most useful spectral wavelengths, prior to aerial data acquisition, would provide a great deal of information to researchers where various film, filter, and date combinations could be used most effectively.

Remote Sensing Considerations in the Eastern Deciduous Forest

Medium to high resolution imagery from aerial and satellite sensors is often used during the validation process for coarse resolution satellite LAI products (Chen *et al.* 2002, Myneni *et al.* 2002). Correlations between LAI and hyperspectral data have demonstrated stronger relationships than broadband multispectral data across several different biomes (Bond *et al.* 2004). Stand-level investigations allow researchers to conduct field studies on manageable plots to ascertain a higher level of detail from imagery products. Although satellite imagery capabilities have improved significantly in the last decade, only aerial imagery can currently provide the high spatial resolution, as well as the multi- and hyperspectral imagery necessary for identifying individual trees. Identification of individual trees can provide a wealth of information, including the detection of rare individuals, genotypes, species, health, recruitment, and change over

time (Key *et al.* 2001, Warner *et al.* 1998). Most importantly, aerial remote sensing provides forest ecologists with a unique image displaying the spatial distribution of individual trees consuming, and competing for, light resources in the upper canopy (Culvenor *et al.* 1998). This partitions the crowns into different dominance classes across a landscape that would otherwise be difficult to map and monitor.

The Eastern Deciduous Forest is a mosaic of many species and represents the most diverse and species-rich forest in North America (Botkin *et al.* 1993). This diversity presents a number of obstacles for remote sensing investigators. The Eastern Deciduous Forest typically exhibits a canopy of varying heights, an irregular array of crowns of differing shapes and sizes, shadowing within crowns, crowns surrounded by erratic shadows, and structural diversity that increases as the forest matures. A number of forest mapping investigations have been focused on coniferous forests and plantations where dark tree shadows and bright tree tops have been exploited to delineate individual trees (Dralle and Rudemo 1996, Gougeon 1997, Pouliot *et al.* 2002, Wulder *et al.* 2000). Methods that exploit crown shape and brightness in relation to shadowing effects have been unsuccessfully applied in deciduous forest ecosystems. Several studies have employed multispectral (Key *et al.* 1998, Key *et al.* 2001) and hyperspectral (Foster and Townsend 2002, Martin *et al.* 1998) sensors to conduct species-level mapping investigations in the eastern deciduous forest. In all of these studies, significant ancillary ground truth data were used to enhance the utility of the remotely sensed data; also, steps were taken to minimize topographic effects in rugged terrain.

Image Classification

Image classification is the process of grouping image pixels into classes that exhibit similar spectral and/or textural values and assigning them to meaningful information classes. Classification methodologies of remotely sensed data can be divided into supervised and unsupervised forms (Fassnacht *et al.* 1997), and may be typified as being of *hard/rigid* classical set theory, or as being of *soft/fuzzy* set theory.

Unsupervised classification algorithms require little or no "*a priori*" knowledge of image features, as information classes are statistically clustered by natural groupings of spectral values in the dataset and labeled "*a posteriori*." The only specifications of unsupervised classifications are the number of desired classes, class convergence thresholds, and the number of iterations to perform. Commonly used unsupervised classification algorithms include ISODATA (Hoover *et al.* 2000) and K-Means (MacQueen 1967).

Supervised classifications require the analyst to collect image training data, create spectral signature data from imagery, or import spectral signature data from laboratory and field measurements. Collecting representative training data can be problematic, because data collected with polygons may be auto-correlated, and also under-representative of informational classes (Campbell 1981, Griffith 1987, Muchoney and Strahler 2002). The collection of single, non-contiguous pixels may provide higher variance than polygonal pixel collection and avoid the associated autocorrelation effects, although it may not be spectrally broad enough to convey informational classes accurately. Examples of commonly used supervised classifications include Parallelepiped (Jain 1989, Jensen 1983), Minimum Distance (Jahne 1991), Mahalanobis

Distance (Richards 1993), Maximum Likelihood (Foody *et al.* 1992, Whitmore *et al.* 1993), Spectral Angle Mapper (Boardman 1995), and Binary Encoding (Mazer *et al.* 1988).

Class selection with image processing classifiers is generally described as *hard/crisp* or *soft/fuzzy* in the partition of feature space into informational classes. All of the classifiers listed above represent hard classifiers. Crisp partitions are characterized as being "mutually exclusive and totally exhaustive" (Congalton 1991), meaning that all pixels within an image are forced and generalized into discrete thematic classes during classification. Classes of crisp partitions are typically unable to accurately convey thematic information to the analyst, because boundaries in nature tend to transition along a gradient. Crisp partitioning becomes further constrained with the introduction of mixed pixels. This occurs when the spectral and/or spatial resolution of the sensor is unable to resolve pixels that contain numerous feature classes, or when adequate spectral or training data are lacking for those classes. The solution to improving classification accuracies with mixed pixels has focused on the use of sub-pixel mixture modeling (Adams *et al.* 1995, Roberts *et al.* 1990, Settle and Drake 1993, Sohn and McCoy 1997) and the use of soft or fuzzy set classifiers (Bastin 1997, Foody *et al.* 1996). Sub-pixel mixture modeling requires a definition of spectral endmembers, and highly calibrated data from a sensor having robust spectral capabilities.

Fuzzy set theory and fuzzy logic were developed as devices for reasoning with imprecise concepts and data in decision processing of complex systems (Zadeh 1965, Zadeh 1973). Because human reasoning is imprecise, fuzzy set theory offers a viable alternative to classical set theory in dealing with real-world problems (Aber *et al.* 2000).

In a binary example of class membership, two simple classes could be defined as 0=water and 1=land, where all pixels must be placed into one of these two classes. When a pixel is composed of equal parts of water and land, homogenization of class features occurs, leading to generalization and misclassification. Conversely, in classification using fuzzy sets, a pixel is assigned an ordinal quantitative membership grade between 0 and 1 for each feature class in the analysis. Adding up these membership grades for all classes of a single pixel yields a total of 1, though if neural networks are employed, the sum may not equal 1 (Foody *et al.* 1996). The closer the membership grade is to 1 for a given class, the more that pixel belongs to that feature class based on the training data provided. The major difference between classical set theory and fuzzy set theory in image processing is that fuzzy sets allow the analyst to produce classifications that discern the identity of mixed pixels having numerous constituent classes. This is possible by providing training data that exhibit substantial overlap between classes to mimic real-world conditions (Eastman and Camm 1995). After fuzzy logic classifications, the analyst often hardens, or *defuzzes*, feature classes by thresholding the membership grades in each feature class to enhance thematic meaning, at the expense of quantitative data (Foody and Trodd 1993).

The use of soft classification has become widespread in image processing of remotely-sensed data as a result of its effectiveness in the discernment of class membership at the sub-pixel level. Soft classifications have provided useful results when data are noisy, display high spatial frequency, exhibit a large degree of within-class variability, or contain a considerable number of mixed pixels (Foody 1999, Foschi and Smith 1997, Lein 2003a). Although many variations of soft classifiers have been

developed and modified for a wide range of applications, the use of the Dempster-Shafer Theory of Evidence has provided an applicable soft classification alternative to fuzzy and Bayesian classifiers.

Dempster-Shafer Theory of Evidence

The Dempster-Shafer Theory of Evidence arose from the evaluation of uncertainty in probabilistic modeling and hypothesis testing (Dempster 1967a, b; Shafer *et al.* 2001). Unlike Bayesian Probability Theory, the Dempster-Shafer method explicitly recognizes that the knowledge base present supporting a hypothesis may be incomplete. Bayesian Probability Theory treats this lack or incompleteness of evidence for a particular hypothesis against it, whereas the Dempster-Shafer method treats this simply as a lack of evidence supporting a hypothesis. The flexibility that the Dempster-Shafer method affords over Bayesian Probability Theory has led to its use in decision analysis of artificial intelligence and expert systems (Shafer *et al.* 2001), and situations where data may be lacking, incomplete, or the analysis is underscored by uncertainty (Caselton and Luo 1992). The use of the Dempster-Shafer method in remotely sensed land use/land cover classifications has outperformed Bayesian classifiers (Le Hegerat-Mascle *et al.* 1997, Le Hegerat-Mascle *et al.* 2000), and has demonstrated its ability to depict complex urban and agricultural landscapes accurately where other classification methodologies were inadequate (Lein 2003a, b).

In this investigation the Dempster-Shafer Theory of Evidence algorithm was applied using the software package Idrisi Kilimanjaro (Clark Labs, Worcester, Massachusetts, USA). In the explanation of underlying facets of the theory, examples from the current investigation will be used to elucidate its applicability. The

implementation of Dempster-Shafer Theory begins with a hierarchical structure of hypotheses known as the frame of discernment, or the decision frame. This analysis is concerned with mapping three singleton classes: [Maple], [Other], and [Shadow]. These three classes form the structure of the decision frame. Evidence is accepted for these three classes, and all possible combinations, forming sets of numerous hypotheses within the decision frame (Table 2). This is necessary, since uncertainty in the data can sometimes support a multi-classed hypothesis when the evidence supplied is unable to further distinguish class membership.

A basic probability assignment (BPA) is determined by the degree to which evidence supports a hypothetical class combination [Maple, Other], but not [Maple] or [Other] as separate classes. These indistinguishable combinations of classes in the BPA are referred to as supersets. The sum of the BPA in the decision frame will always be equal to 1.0. This means that the ultimate superset of [Maple, Other, Shadow] will equal the complement of the sum of all other classes in the BPA. These numerical values, assigned to each class in the BPA, represent ignorance. Ignorance is defined as the inability to determine any degree of differentiation between classes in the decision frame.

Belief represents the degree to which evidence provides concrete support for class membership through the BPA. Belief for [Maple, Other] equals the sum of [Maple, Other], [Maple], and [Other]. The degree to which a hypothesis cannot be disbelieved is known as plausibility. Plausibility represents the degree to which evidence seems to satisfy the hypothesis, even when hard evidence is lacking to support definitive class membership. In this context, belief represents the lower boundary of the commitment in class membership; plausibility represents the upper boundary. The range established

between these two measures is the belief interval, and represents the degree of uncertainty in class membership within the decision frame. In the analysis for this thesis, belief surfaces have been produced from image data. They provide concrete evidence of class membership based on the signature training data. Using plausibility may have produced surfaces that overstep the limitations of the data set, and display larger errors of commission.

Chapter 3

Site Description

The Black Rock Forest (BRF) is a research site and educational facility located in Orange County, NY, near the town of Cornwall-On-Hudson (Figure 1.0, 1.1). The site is composed of temperate mixed-deciduous species and is located within the Cascade Brook Watershed of the Hudson Highlands Ecoregion. The Black Rock Forest was established in 1927. A brief summary of site characteristics are provided below; it derives from primary literature (Turnbull *et al.* 2002, Tyron 1930). The geographic coordinates of the study area are 41° 24' N, 74° 01' W. Relief at the forest varies from 110-450 m above mean sea level. The region exhibits a humid continental climate, with 1,190 mm average annual precipitation and air temperatures ranging between –2.7 - 23.4°C. The site was previously glaciated; its soil contains glacial till and granite gneiss bedrock.

This investigation focuses on the lower mesic site of the Cascade Brook Watershed, detailed in a previous study and summarized below (Turnbull *et al.* 2002). This site exhibits a basal area of 24.9 m^2 ha^{-1} with an average of 650 trees per hectare (Table 1). Canopy height at the site varies from 20 – 30 m with canopy gaps being exploited by *A. rubrum*. Tree counts and basal area measurements indicate that *Q. rubra* had the greatest contribution to basal area, although there are more stems represented by *A. rubrum* and *Betula alleghaniensis* Britt. (yellow birch). The overstory is dominated by *Q. rubra* and *A. rubrum*. The understory is primarily represented by *A. rubrum*, *A. saccharum* L. (sugar maple), and *B. alleghaniensis*. *Q. prinus* was limited in its distribution to small microsites of higher topography.

Chapter 4

Materials & Methods

Leaf Litter/Leaf Area Measurements

Leaf litter and leaf area measurements were obtained in the methods displayed in the flowchart diagram Figure 4.0. Kim J. Brown conducted all leaf litter and leaf area measurements during the autumn of 2000. Specific leaf area (SLA) was determined by collecting approximately 100 leaf samples per species at the end of the growing season, when the leaves were still green but fully formed. Individual leaf areas were measured while the leaves were fresh using the LI-3100 portable leaf area meter (Li-Cor Inc., Lincoln, Nebraska, USA). The leaves were dried for over 48 hours at 60° C, and their mass was weighed to the nearest 0.01 g. A regression relationship was determined for each species (red maple, chestnut oak, red oak) where SLA is the slope term of mass (x-axis) versus area (y-axis).

Leaf area was measured through the use of leaf litter traps at both an upper xeric site and a lower mesic site throughout the autumn of 2000. Each research site was composed of a 50 m^2 plot, which was segmented into twenty-five 10 m^2 plots per site. A random numbers table was used to select six 10.0 m^2 plots at each site. Each plot was equipped with a 0.36 m^2 netted leaf litter trap. The leaves were collected in leaf litter traps from September 30, 2000, through November 15, 2000 and were emptied six times throughout this 46-day period of autumnal leaf fall. Leaves from traps were sorted according to species and placed into four classes: *A. rubrum*, *Q. prinus*, *Q. rubra*, and

other species. Leaves were dried for over 48 hours at 60° C, and their mass was weighed to the nearest 0.01 g.

LAI_{SPP} was calculated using both the SLA regression relationship and the species-specific leaf masses collected in leaf litter traps. Species leaf area was estimated from leaf mass collected in leaf litter traps, and divided by the size of the leaf litter trap. The LAI_{SPP} information is tabulated in Table 3.

Image Acquisition

A specially designed digital imaging system was used for branch- and canopy-level data collection. This system provided flexibility during data acquisition under adverse weather conditions and at multiple spatial scales. This digital imaging system was designed by Milton Smith at the University of Washington and operated by Stephanie A. Bohlman and Kim J. Brown at BRF. Imagery was collected on June 21, 2000, and June 23, 2000 during overcast conditions to avoid the harsh shadowing effects of sun angle. The imaging system consisted of six Marshall Electronics V-1050A CCD cameras (Marshall Electronics, El Segundo, California, USA) outfitted with Rainbow Optics fixed focal length lenses (Rainbow Optics, Castro Valley, California, USA). The lenses were equipped with Thermo Oriel (Thermo Oriel, Stratford, Connecticut, USA) and Edmund Optics (Edmund Optics, Barrington, New Jersey, USA) narrow bandpass filters that permitted EMR to enter the camera in the VIS and NIR mean wavelengths of 480 nm (blue), 550 nm (green), 676 nm (red), and 730 nm, 850nm, and 940 nm (NIR), respectively. Images acquired with this system are formatted as a set of six 314 x 234 pixel images, or one image/wavelength. The images require extensive manual co-registration of image features to create multispectral data sets.

Branch-Level Spectral Analyses

The methods employed in the branch-level spectral analyses are displayed in flowchart diagram Figure 4.1. A large bi-colored panel with both specular and blackbody surfaces was placed in each remotely-sensed scene to act as a static control measure in spectral calibration. Gail Yamada at the University of Washington Geology Remote Sensing Lab measured the reflectance properties of the calibration panel using a PerkinElmer Lambda 19 Spectrometer (PerkinElmer, Wellesley, Massachusetts, USA). The empirical line method was used to convert the raw radiance digital number (DN) image data to true reflectance (Leckie *et al.* 1999). Previous studies in which this method of calibration have been used have achieved results with minimal errors of several percent (Leckie *et al.* 1999, Price 1995).

Branch-level images were obtained for *A. rubrum*, *Q. prinus*, and *Q. rubra* (Figure 4.2). These images were acquired using a cherry picker equipped with a 20.0 m boom and the imaging system positioned 5.0 m above the surface of the crown. The image sets were mosaicked using Adobe Photoshop (Adobe Systems Incorporated, San Jose, California, USA). Pixel scaling varied by image set, with pixel sizing of *A. rubrum* at 1.3 cm^2, *Q. prinus* at 0.8 cm^2, and *Q. rubra* at 1.2 cm^2. The size of the sample frame was chosen to simulate the sensing of several leaves, and then also a much larger aggregate of leaf layers. Branch images for *Q. prinus* varied in scale, since the imaging system was much closer to the canopy. This reduced the path length between canopy and the imaging system increasing the size of the pixel. Samples from *Q. prinus* images were visually assessed in order to represent a spatial area similar to the other species sampled.

A one-way analysis of variance (ANOVA) was performed on the branch-level data to calculate significant spectral differences between species (Table 4).

Canopy-Level Spectral Analyses

The methods used in the canopy-level analyses are displayed as a flowchart in Figure 4.3. Canopy images were obtained with the imaging system mounted on a Bell 206 Jet Ranger Helicopter (Bell Helicopter Textron, Hurst, Texas, USA). A laser altimeter and airborne GPS were used in the helicopter to ensure that image sets were acquired 76.0 m above the canopy. Helium balloons were used to identify both the research sites from the helicopter, and also guide image acquisition at the intended locations. Mosaicking the co-registered multispectral images in a seamless format was impossible, due to the small image footprint acquired and an inherent parallax introduced by the design of the imaging system.

The green band (550 nm) provided an image free from camera and lens effects observed in other images. The 550 nm images also exhibited distinct differences in canopy brightness for different species identified at the site. In addition, this wavelength possessed a wide range of DN values for one image band (0-97). The green band was mosaicked in Adobe Photoshop with sequential adjacent images in order to produce a 250 by 250 pixel image of the lower site surrounding the canopy tower (Figure 4.4). Gaussian smoothing was performed in ENVI (Research Systems Inc., Boulder, Colorado, USA) to remove any artifacts from the mosaicking process.

This gaussian smoothed image was then imported into Idrisi Kilimanjaro for image classification. Access to a unique array of non-traditional fuzzy and soft classifiers led to the selection of the software package Idrisi Kilimanjaro for image processing.

Supervised training data for *A. rubrum* [Maple], *Q. rubra* [Other], and [Shadow] were collected with the MAKESIG module at an area surrounding the lower research canopy tower (Figure 4.5). The signature data are generalized into these three classes for two reasons: (1) in order to make comparisons with the LAI_{SPP} information, and (2) because the spectral data needed to discern more feature classes are lacking. The signature training data statistics indicate that the [Shadow] class DN values range from 0-18, the [Other] class DN values from *Q. rubra* crowns range from 10-61, and the [Maple] class DN values obtained from *A. rubrum* crowns range from 24-94.

The BELCLASS classification algorithm was used to create belief surfaces in this research project. This algorithm is based on the variant of Bayesian Probability Theory known as the Dempster-Shafer Theory of Evidence. Belief surfaces were produced for this study in order to evaluate the degree to which available signature training data provides concrete support for a hypothesis.

It was necessary to evaluate and classify the BELCLASS surfaces by hardening the belief surfaces into a single map product. Belief surfaces were hardened using the MAXSET algorithm. Although the MAXSET algorithm requires training data, it acts more like an unsupervised classifier, since it can assign a pixel to a class that lacks exclusive training data. This algorithm evaluates the surfaces, assigning each pixel to a class based on two determining factors: (1) the greatest degree of belief present within a belief image set, and (2) the training signature data. The classes generated from MAXSET take into consideration all possible permutations from different class combinations, within the Dempster-Shafer Theory of Evidence hierarchy (Table 2). The resulting surface created is called the maximum basic probability assignment

classification. The maximum basic probability assignment from MAXSET represents indistinguishable combinations of classes based on the training data provided.

Interpretation of the MAXSET combination [Shadow, Maple] can be interpreted as support for [Shadow], support for [Maple], or support for [Shadow, Maple] with the algorithm unable to determine class membership based on the evidence available. These indistinguishable combinations of classes are known as supersets; they occur from ambiguous signatures, or the presence of a mixed class in the data set (Eastman and Camm 1995).

Three soft classification approaches using the BELCLASS and MAXSET algorithms were performed in this study. The approaches differ from one another according to two factors: (1) whether the probability values assigned to the training data in BELCLASS were equal or specified based on other informational sources (2) whether BELCLASS surfaces or probability values were used to drive MAXSET.

In Approach 1, MAKESIG signature training data for the feature classes [Shadow], [Maple], and [Other] were collected (Figure 4.5). These data were entered as signatures into the BELCLASS decision frame and assigned equal probability values split between the three feature classes (a 33.3 % probability for each class). The BELCLASS surfaces produced include [Maple] (Figure 4.6), [Other] vegetation (Figure 4.7), and [Shadow] (Figure 4.8). Values closer to 1.0 indicate a high degree of belief, whereas values closer to 0.0 indicate a low degree of belief for a feature class based on the training data available. In addition to the surfaces produced from the signature files, each BELCLASS analysis is accompanied by a surface of classification uncertainty (Figure 4.9). This image expresses ignorance that evidence does not support the hypothesis that a

pixel belongs to any of the classes in the classification. The BELCLASS surfaces were entered into MAXSET and given equal probability values in order to produce a maximum basic probability assignment classification (Figure 4.10).

The BELCLASS surfaces of [Other] and [Maple] from Approach 1 were used as inputs for MAXSET in Approach 2. The [Shadow] surface was replaced by a probability value extracted from the Approach 1 MAXSET result for [Shadow] (15.83 %). The MAXSET maximum basic probability assignment yielded a classification with the three feature classes of interest and one mixed superset (Figure 4.11).

Approach 3 used the MAKESIG signature training data and productivity values observed in the LAI_{SPP} information to drive BELCLASS and MAXSET. To accomplish this, the LAI_{SPP} information (Table 3) was generalized to match feature classes detectable with the canopy-level remote sensing data. This comparison was made possible by collapsing the LAI_{SPP} information into [Maple] and [Other]. The values obtained from the LAI_{SPP} information indicate that the [Maple] feature class represents 39 % of the productivity at this site, and [Other] represents 61 % of the remaining productivity. These percentages in productivity were substituted as probability values in BELCLASS and MAXSET for [Other] and [Maple]. The probability value for [Shadow] was extracted from Approach 1 at a value of 15.83%. Prior to entering the [Other] and [Maple] probability values into BELCLASS and MAXSET, it was necessary to account for the percentage of [Shadow] and multiply the LAI_{SPP} percentages by the remaining number of vegetated pixels in the image. This forced the data into classes based on the generalized LAI_{SPP} information. The resulting maximum basic probability assignment yielded an image composed of the three feature classes of interest (Figure 4.12).

Chapter 5

Results & Discussion

Branch-Level Spectral Analyses

Significant spectral differences ($\alpha < 0.05$) at the branch-level were detected between *A. rubrum*, *Q. prinus*, and *Q. rubra* at both sampling scales and at all six wavelengths examined in this study (Table 4). Three sample measurements were not plotted due to erroneous data values obtained after the empirical line calibration was performed. These errors were identified on samples of *Q. rubra* at 480 nm and 676 nm, and on samples of *Q. prinus* at 850 nm. Reflectance values for *Q. rubra* were below 0% reflectance at 480 nm and 676 nm. The blue and red wavelengths where this was observed in the *Q. rubra* samples are regions of the spectrum characterized by high levels of absorption by photosynthetic pigments. In the sampled images the foliage is extremely dark indicating strong absorption features. The *Q. prinus* samples at 850 nm exhibited reflectance values over 100%. The NIR wavelengths in this region of the spectrum are either reflected or transmitted by vegetation. In a review of the image sampled, the adaxial surfaces of leaves in the upper crown of *Q. prinus* trees exhibited a highly specular reflectance at 850 nm.

The erroneous data values observed in several sampled wavelengths indicated that the spectral properties of the reflectance panel were limiting and did not span the effective range necessary to achieve a proper calibration. Reflectance from other scene elements may have corrupted the integrity of reflectance values used in calibration or vegetation sampling. This effect was minimized through the careful selection of branch-

level images that did not contain areas of bare soil, rocks, or reflectance from the boom or base of the cherry-picker.

The crown and branch morphology for *A. rubrum* and *Q. rubra* facilitated the sampling methods presented here. However, the clumpy foliage distribution and open crown morphology of *Q. prinus* made it difficult to make comparisons between all three species using the same methods. The *Q. prinus* images were characterized by large within-crown gaps. Images for *Q. prinus* were acquired at a higher resolution than other species sampled, and the calibration panel was located on the forest floor versus in the upper canopy. The higher resolution properties can be attributed to the clumpy distribution of foliage. As branches escalated in the crown, the path length between the camera and foliage decreased, skewing the scale across the image. *A. rubrum* and *Q. rubra* displayed a more even distribution of foliage allowing the calibration panel to be placed in the upper crown. The location of the calibration panel on the forest floor for *Q. prinus* images made it hard to eliminate the possibility that boom and soil reflectance influenced the reflectance values obtained. The decreased EMR reaching the lower canopy may have been an additional factor influencing the spectral calibration.

LAI_{SPP} Measurements at Black Rock Forest

In the year 2000, the measurements of LAI at the low, mesic site at BRF indicated that this plot had an LAI value of 5.89, while the upper, xeric site had an LAI value of 4.18 (Table 3). The differences in productivity between these two contrasting sites will not be discussed in this analysis, as this investigation focused on the lower, mesic site. The LAI data for the high, xeric sites represents a valuable information source that is

included in this paper as a reference for other studies and to display the variability in species-level productivity at BRF.

The results indicated that there are large differences in productivity observed for species at this site when measured with the LAI_{SPP} metric. *A. rubrum* had an LAI_{SPP} value of 2.32 and represented 39% of the total productivity. *Q. rubra* had an LAI_{SPP} value of 2.10 and accounted for 36% of productivity at the plot, while *Q. prinus* had an LAI_{SPP} value of 0.17 and represented 3% of the total productivity. The other species had a combined LAI_{SPP} value of 1.3 and represented 22% of the productivity.

To make comparisons between the image classification results and plant productivity measurements, it was necessary to generalize the LAI_{SPP} information. The LAI_{SPP} fractions of *Q. prinus*, *Q. rubra*, and other species were added together to create the [Other] vegetation class. The class combination resulted in 39% of the LAI being represented by *A. rubrum* [Maple] and 61% of the LAI represented by [Other] species in the study area. The purpose of this method was to isolate *A. rubrum* from all other species in the study area and to facilitate the image classification using one spectral wavelength. In comparing the LAI information with percentages of vegetation cover derived from image classifications, this method assumes that all species are represented in the upper canopy where they can be measured using remotely sensed methods.

Canopy-Level Spectral Analyses

The methods used in Approach 1 represent the least amount of analyst intervention in the classifications produced in this study. In BELCLASS and MAXSET the surfaces created were given equal probability values. Five classes were produced from MAXSET (Figure 4.10), the three original feature classes [Other], [Maple], and

[Shadow] as well as two indistinguishable supersets [Maple, Other] and [Other, Shadow]. The [Shadow] class is of critical importance in all of the approaches used in this investigation. [Shadow] accounted for 15.83% of the image in this analysis. To compare the percentages of canopy cover obtained with these classification methods and the LAI_{SPP} information, the number of [Shadow] pixels must be subtracted from the pixels classified as vegetation. The elimination of the [Shadow] class from the total number of pixels resulted in the following class membership contributions: [Other] (42.93%), [Maple, Other] (17.22%), [Maple] (37.22%), and [Other, Shadow] at (2.61%).

The superset of [Maple, Other] represented a challenging classification problem. The 17% of vegetation cover that is shared between the confused superset of [Maple, Other], is a result of overlapping DN values that exist in the signature training data. Pixels for the [Maple, Other] class are found on the periphery of areas surrounding [Maple] and [Other] classes. With such a large percentage of the pixels falling into an ambiguous class it made it difficult to draw definitive conclusions from this classification. The superset [Other, Shadow] represented a much smaller percentage of the total scene (2.61%). The lack of a [Maple, Shadow] superset indicated that the spectral properties for these two classes differed enough to avoid confusing the classifier. A comparison between the vegetation class membership results with the LAI_{SPP} information indicated that [Maple] was underestimated by 1.78% and [Other] was underestimated by 18.07%. This classification method did not produce classifications reflecting productivity values observed with the LAI_{SPP} information and exhibits misclassifications of feature class membership.

Approach 2 was similar to Approach 1, in that equal probability values were applied to the signature training data to create BELCLASS surfaces. The results from the MAXSET classification produced four feature classes that are displayed in Figure 4.11. The class membership statistics were calculated and prior to the removal of the [Shadow] class, this class accounted for 13.71% of the image. The probability value used for the [Shadow] class in MAXSET was slightly higher than this at 15.83%. When the [Shadow] class is accounted for and subtracted from the analysis, the recalculated statistics for vegetation cover indicated that the [Other] class covered 55.35% of the image. The [Maple] class accounted for 40.91% of the classification. The superset of [Other, Shadow] accounted for the remaining 3.73% of the image. Comparing the vegetation class membership results with the LAI_{SPP} information indicated that the [Other] class was underestimated by 5.65% and the [Maple] class was overestimated by 1.91%.

This approach differs from the other methods through its explicit use of probability values and training signature data as inputs into BELCLASS. The results from this MAXSET classification produced three classes that are displayed in Figure 4.12. Prior to the removal of [Shadow], this class accounted for 12% of the image. The probability value used in MAXSET for [Shadow] was 15.83%. After the removal of the [Shadow] class, the [Maple] class accounted for 42% of the coverage, and the [Other] class represented the remaining 58% of the image. Comparing the classification results with the LAI_{SPP} information, the [Maple] class was overestimated by 3%, while the [Other] class was overestimated by 3%.

Comparisons of Image Classification Results With LAI

In all of the image classification approaches tested in this investigation, the values obtained for the [Other], and [Maple] classes did not match the observed productivity values of the LAI_{SPP} information. Some of the classifications produced percentages of cover for [Maple] and [Other] that approached the observed LAI_{SPP} values. However, all of the classifications produced in this investigation displayed evident classification errors and lacked a field verification to assess the accuracy of the classification results. The classification errors can be identified by comparing the areas where signature data was collected on species of known identity (Figure 4.5) and the classifications produced in this investigation (Figure 4.10, 4.11, 4.12).

It was difficult for BELCLASS to discern areas in the upper canopy where the brightness of some *Q. rubra* crowns [Other] exhibited high DN values that overlapped with signature training data for *A. rubrum* [Maple]. It was also difficult for BELCLASS to detect *A. rubrum* emerging from gaps in the canopy, where the lower DN values on the edges of the crowns were more characteristic of the [Other], and [Shadow] signature training data. The spectral overlap between [Other] and [Shadow] made it difficult to discern class membership for these classes, where foliage in the lower canopy was often misclassified.

The classification errors identified that there was an apparent lack of spectral information to consistently and accurately detect [Maple]. Conducting the investigation with one spectral wavelength (550 nm) did not make it possible to separate feature classes that displayed overlapping DN values. The BELCLASS algorithm, with its base in Dempster-Shafer Theory, was selected for this investigation due to its ability to be

used on data sets where evidence is lacking, incomplete, or underscored by uncertainty. In this investigation, the lack of spectral data made it impossible to produce remotely sensed estimates of canopy cover for *A. rubrum* that reflected the forest composition identified with the LAI_{SPP} information.

Chapter 6

Conclusion

The two objectives of this research were: to determine (1) whether spectral differences exist at branch-level between the oak and maple groups at this site, and (2) whether remotely sensed canopy-level classifications are able to produce estimates of canopy cover for red maple that reflect the forest composition identified with the LAI_{SPP} information.

Significant spectral differences ($\alpha < 0.05$) were observed at the branch-level between *Acer rubrum* (red maple), *Quercus prinus* (chestnut oak), and *Quercus rubra* (red oak). This analysis was conducted in June, 2000 using an experimental digital imaging system with six wavelengths of EMR at 480 nm (blue), 550 nm (green), 676 nm (red), and 730 nm, 850nm, and 940 nm (NIR), respectively. The results from this investigation are critical for future remote sensing investigations in mixed-oak forests, where dynamic changes in species composition are occurring. The fact that these three species can be spectrally detected with discrete, multispectral, wavelengths at the branch-level indicates that species mapping at the canopy-level may be possible. A similar research project adapting the techniques presented in this investigation may allow for the spectral detection of these species in other mixed-oak forests.

Multispectral canopy-level data was acquired in June 2000 at Black Rock Forest, NY. The 550 nm (green) wavelength was selected to create maps of canopy cover for *A. rubrum* and other species at a mesic site at Black Rock Forest, NY. The lack of multiple spectral wavelengths to conduct image classification led to the selection of the BELCLASS algorithm for image classifications. BELCLASS acts as a soft classifier and

is a variant of the Dempster-Shafer Theory of Evidence. This classifier was selected for its ability to produce meaningful classifications when evidence is lacking, incomplete, or underscored by uncertainty. Species-specific leaf area index (LAI_{SPP}) obtained from autumn 2000 leaf litter data were used to produce maps of canopy cover between maple and other species at the site. Three approaches to image classification were conducted, but the lack of spectral information and lack of field verifications produced classifications of questionable accuracies. In all three approaches, the spectral overlap between feature class signatures produced evident classification errors. Due to these conditions, it was not possible to produce accurate estimates of canopy cover for red maple that reflect the forest composition identified with the LAI_{SPP} information.

Initially, this investigation was going to conduct an integrated multi-scale analysis collecting and calibrating multispectral imagery data at the level of the leaf, branch, and canopy. Several unforeseen factors in this project negatively affected the scope of this investigation. At the canopy- and branch-level, issues with imaging system optics and parallax, as well as the size and placement of calibration panels became insurmountable problems to conducting the initial investigation. Leaf-level reflectance data could not be integrated into this study, due to the low sample sizes measured. Several reflectance data values at the branch-level data could not be used, due to the inability of the calibration panel to span the effective spectral range recorded for several samples. Differences in scale for images at the branch-level also made area-based sampling difficult based on the fluctuating path lengths between the imaging sensor, the foliage being sensed, and the location of the spectral calibration panel. Since this investigation the imaging system has been redesigned and consists of one camera body utilitizing a series of filters on a

rotating disc. Although this prevents immediate, simultaneous data acquisition, the final image sets require minor mosaicking efforts in comparison to the methods presented here. If these obstacles are recognized and accounted for in future remote sensing data collections, the setbacks outlined here can hopefully be avoided.

	Lower Site				Upper Site				Forest-wide			
Species	Density (stems ha^{-1})	Density Fraction	Basal Area (m^2 ha^{-1})	Basal Area Fraction	Density (stems ha^{-1})	Density Fraction	Basal Area (m^2 ha^{-1})	Basal Area Fraction	Density (stems ha^{-1})	Density Fraction	Basal Area (m^2 ha^{-1})	Basal Area Fraction
Acer rubrum (Red Maple)	190	0.292	7.9	0.317	110	0.145	0.6	0.025	227	0.309	1.6	0.076
Quercus prinus (Chestnut Oak)	30	0.046	1.5	0.060	390	0.513	15.7	0.665	133	0.181	5.0	0.238
Quercus rubra (Northern Red Oak)	100	0.154	10.3	0.414	170	0.224	4.8	0.203	168	0.229	8.9	0.424
Other (32 spp.)	330	0.507	5.2	0.209	90	0.118	2.5	0.106	206	0.281	5.5	0.262
Total	650		24.9		760		23.6		734		21	

Table 1. Basal area and stem density at Black Rock Forest, NY (Turnbull *et al.* 2002).

[A]	[Shadow]
[B]	[Maple]
[C]	[Other]
[A, B]	[Shadow, Maple]
[A,C]	[Shadow, Other]
[B,C]	[Maple, Other]
[A, B, C]	[Shadow, Maple, Other]

Table 2. Combinations of classes in the Dempster-Shafer Theory of Evidence decision frame.

Species	Lower Site LAI	Lower Site Fraction	Higher Site LAI	Higher Site Fraction
A. rubrum (Red Maple)	2.32	0.39	0.05	0.01
Q. prinus (Chestnut Oak)	0.17	0.03	1.82	0.43
Q. rubra (Northern Red Oak)	2.10	0.36	1.55	0.37
Other (32 spp.)	1.30	0.22	0.77	0.18
Total	5.89		4.18	
5.03 = Total LAI for the Cascade Brook Watershed				

Table 3. 2000 LAI_{spp} leaf litter trap data from the Cascade Brook Watershed of Black Rock Forest, NY.

BRANCH

10 x 10 pixels (n=100)	*A. rubrum*	*Q. prinus*	*Q. rubra*	*P*-Value
480	2.896 a (.052)	5.655 b (.044)		<.0001
550	15.215 a (.132)	12.110 b (.057)	12.675 c (.170)	<.0001
676	4.810 a (.075)	6.469 b (.079)		<.0001
730	61.066 a (.492)	75.586 b (.914)	45.335 c (.316)	<.0001
850	61.849 a (.502)		52.688 c (.299)	<.0001
940	62.750 a (.407)	83.569 b (1.055)	52.636 c (.411)	<.0001

33 x 33 pixels (n=1089)	*A. rubrum*	*Q. prinus*	*Q. rubra*	*P*-Value
480	2.522 a (.014)	5.634 b (.020)		<.0001
550	14.078 a (.050)	11.724 b (.029)	9.537 c (.068)	<.0001
676	4.690 a (.019)	6.934 b (.036)		<.0001
730	57.905 a (.194)	76.854 b (.260)	38.944 c (.127)	<.0001
850	62.467 a (.182)		45.849 c (.132)	<.0001
940	63.811 a (.175)	86.144 b (.284)	45.111 c (.160)	<.0001

Table 4. Mean branch-level reflectance with results from One-Way ANOVA analyses (±SEM). Different letters within rows indicate statistically significant values at $\alpha < 0.05$ using the least significant difference test of treatment means.

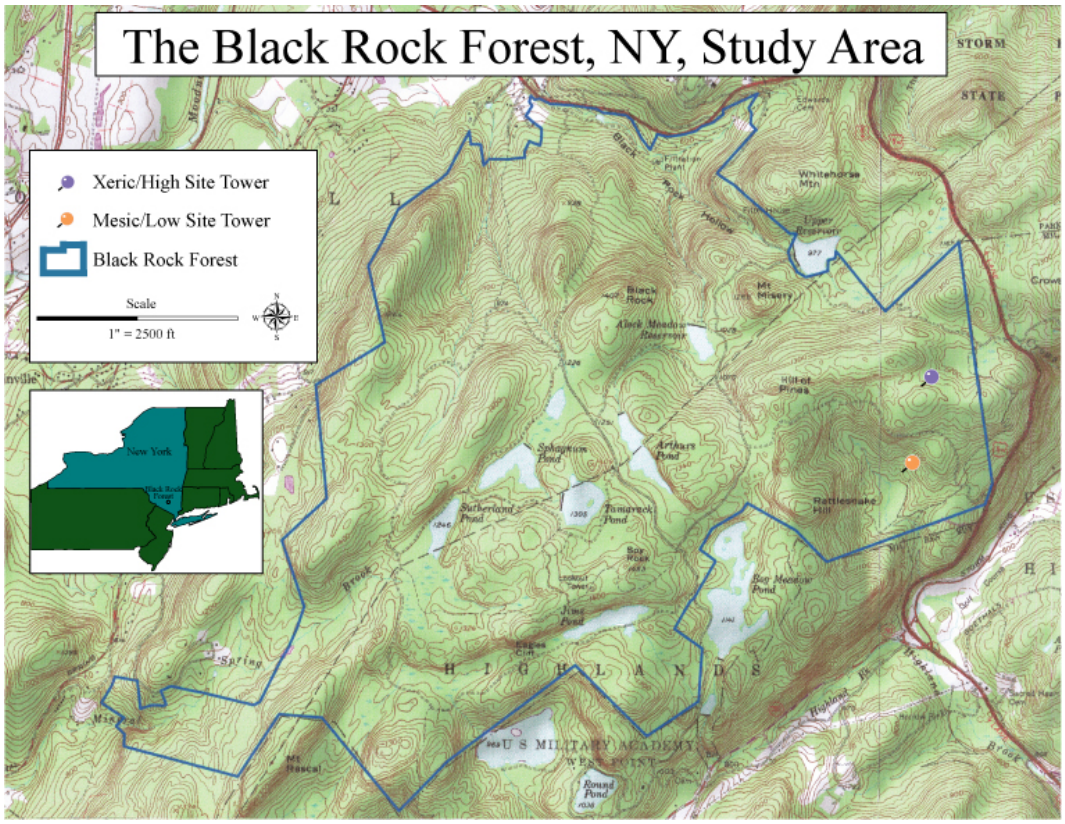


Figure 1.0 Topographic map of the Black Rock Forest. It must be noted that the boundary files used in this document are generalizations and are to be used strictly as a reference for the reader. These maps do not constitute a professional survey, legal demarcation, or declaration of ownership.

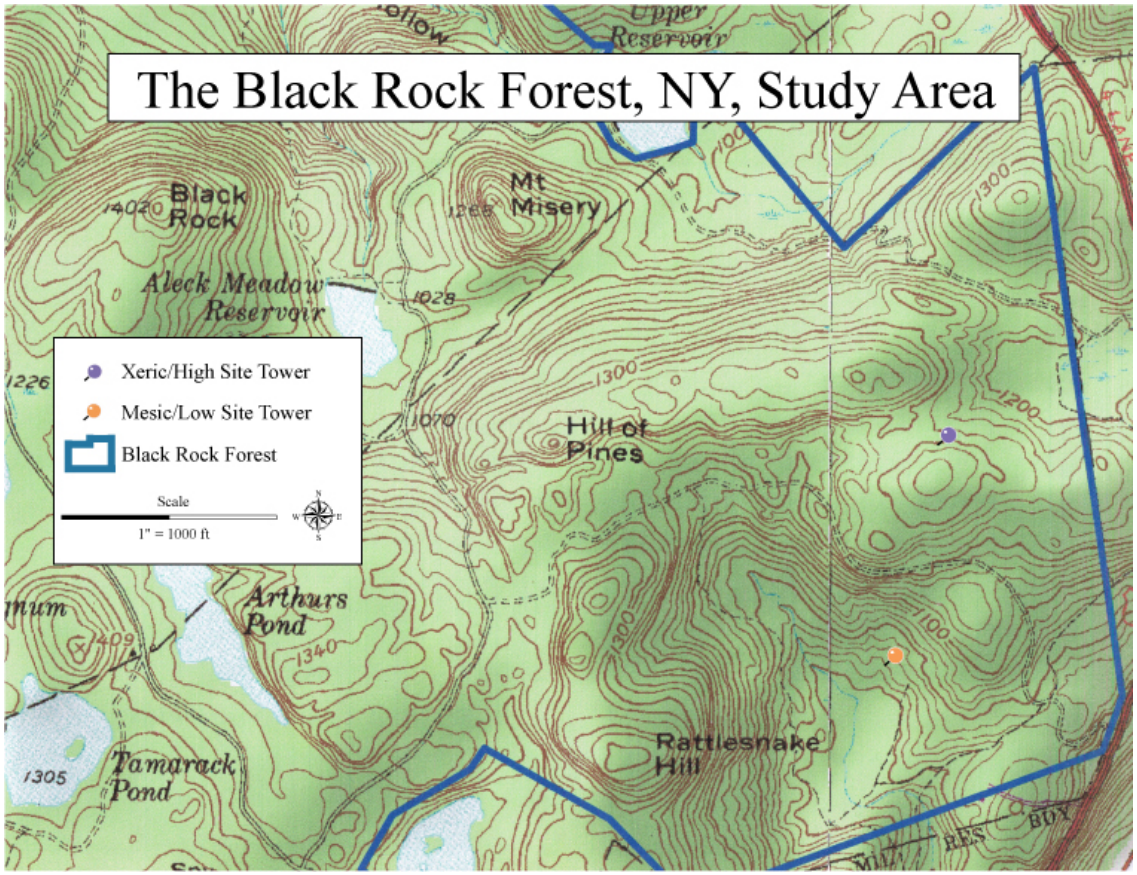


Figure 1.1 Zoom scale topographic map of the study areas at Black Rock Forest.

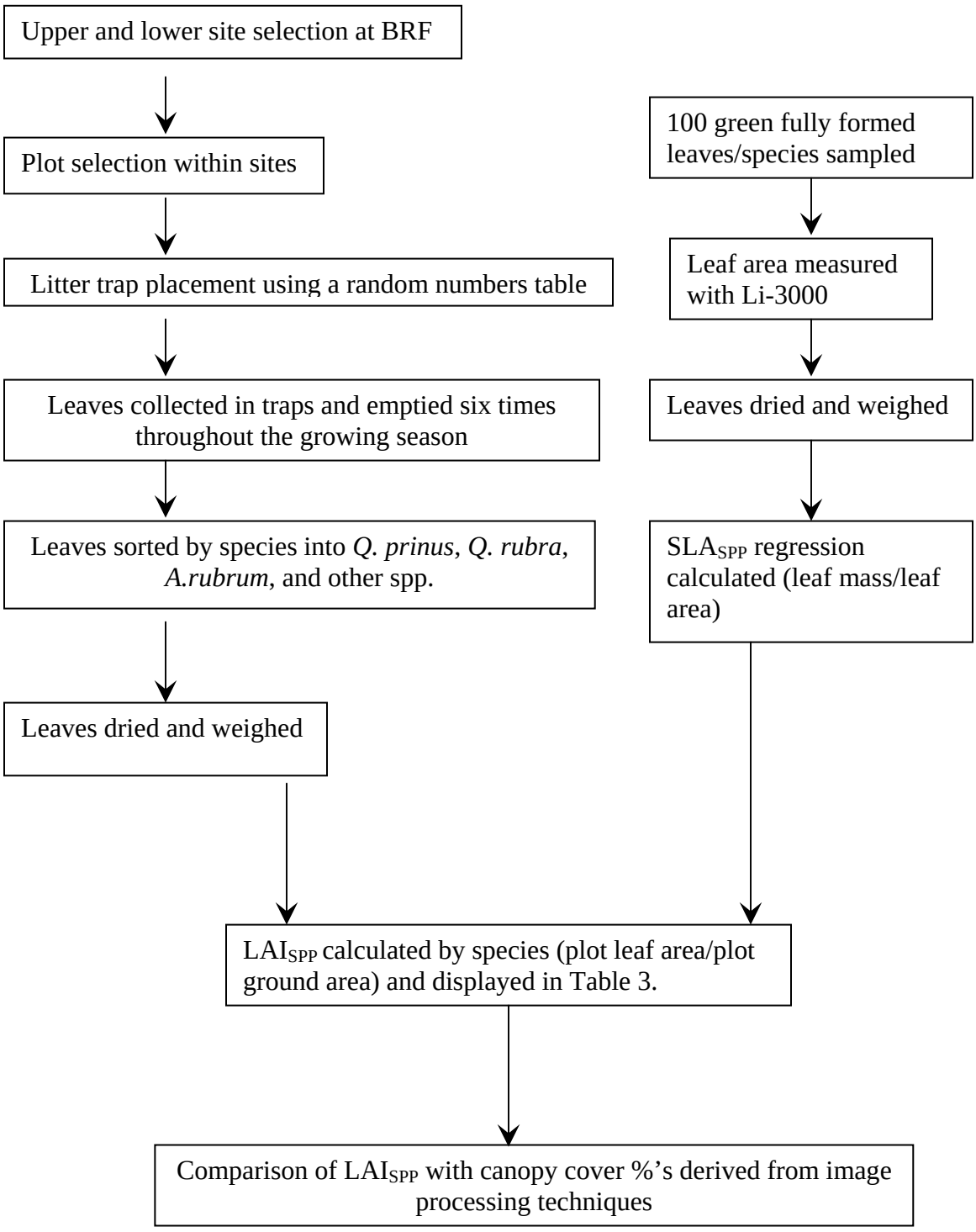


Figure 4.0 Methods flowchart of leaf litter collection and LAI_{SPP} calculation.

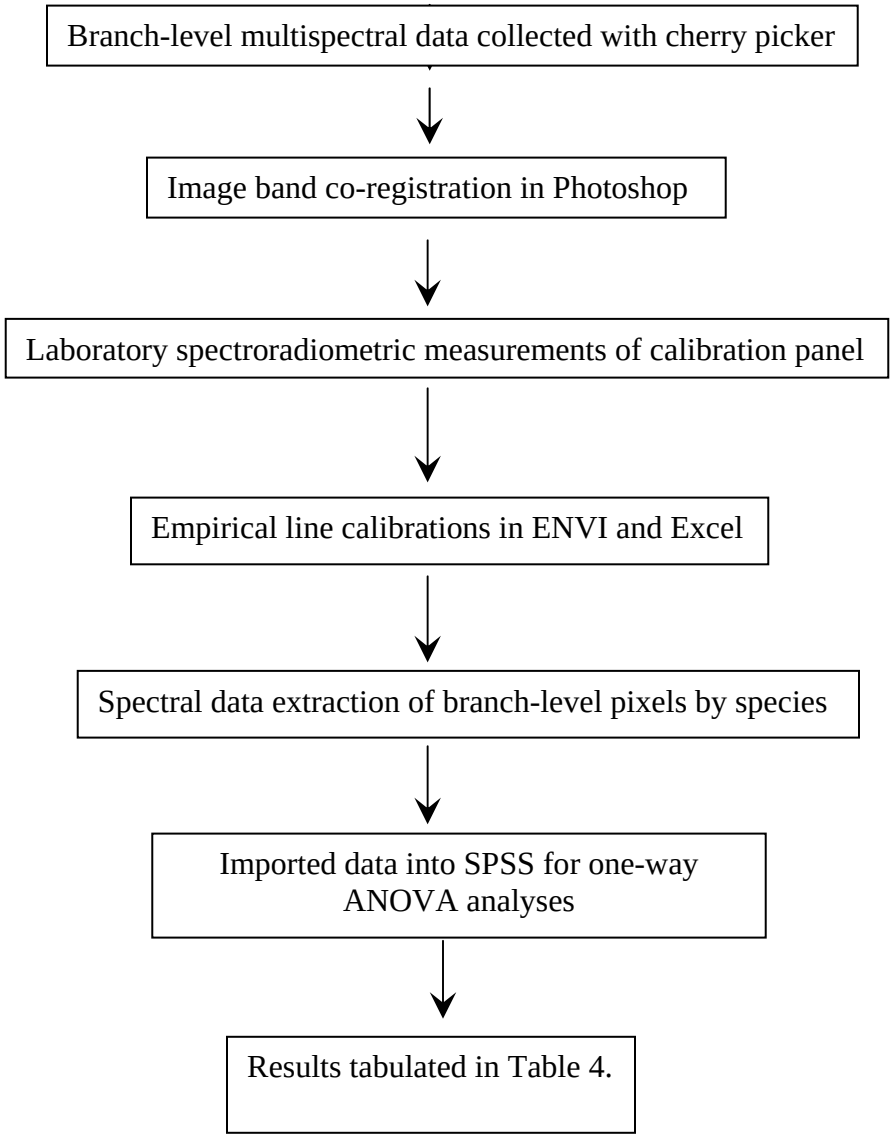


Figure 4.1 Methods flowchart of branch-level spectral analyses.

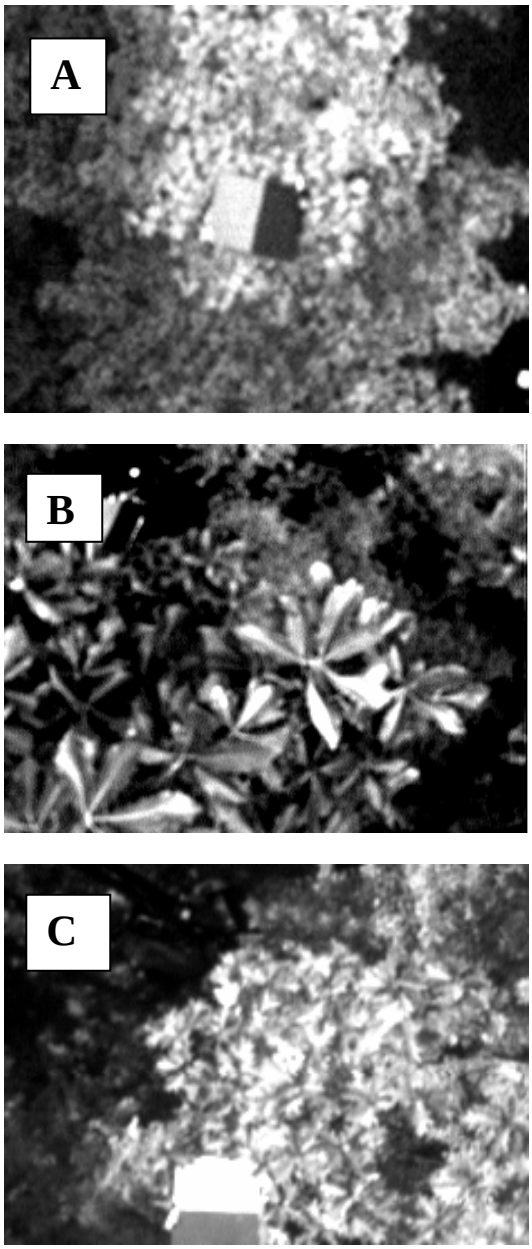


Figure 4.2 Branch-level images from the cherry picker of *A. rubrum* (A), *Q. prinus* (B), and *Q. rubra* (C).

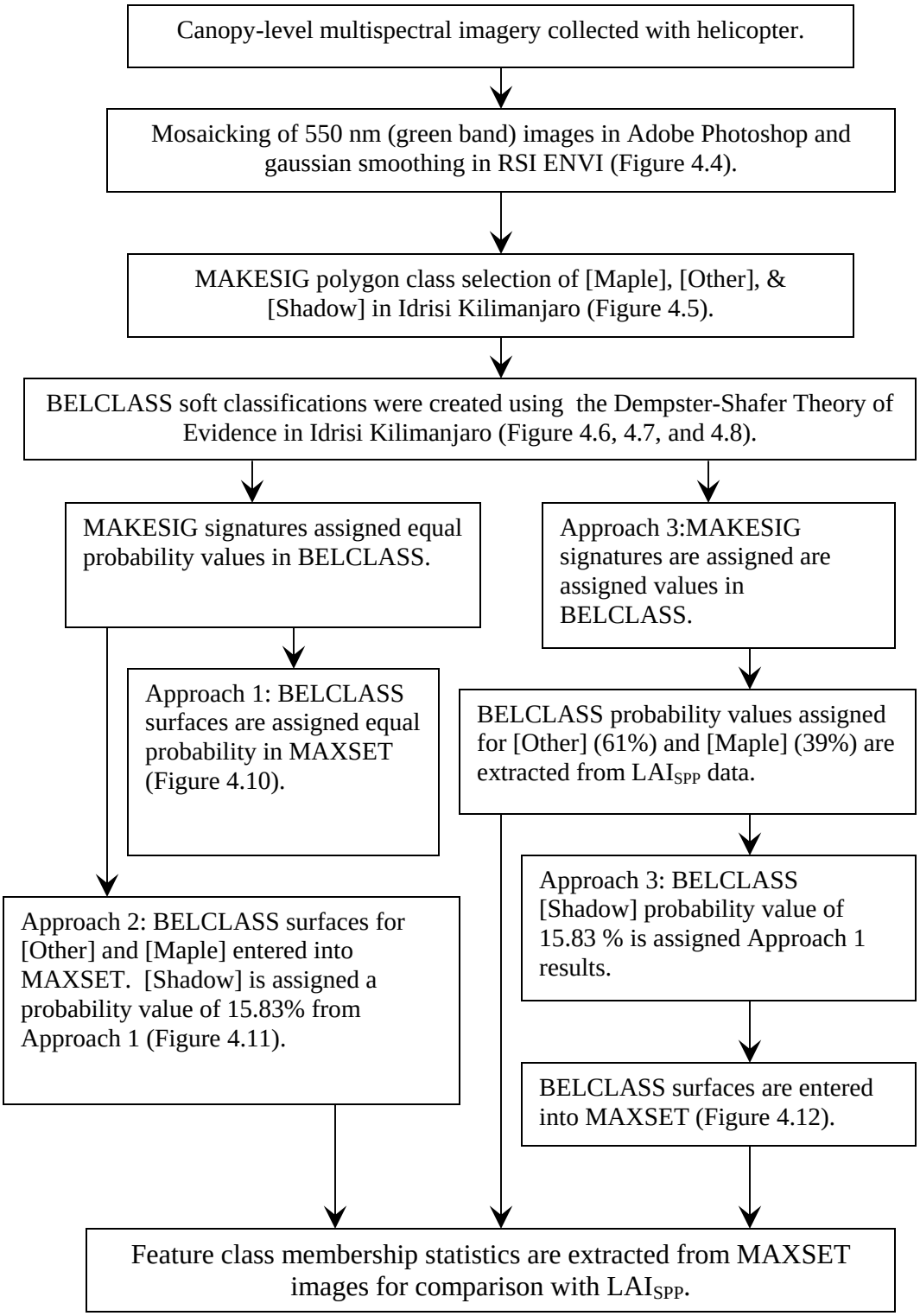


Figure 4.3 Methods flowchart of canopy-level data acquisition and image processing.

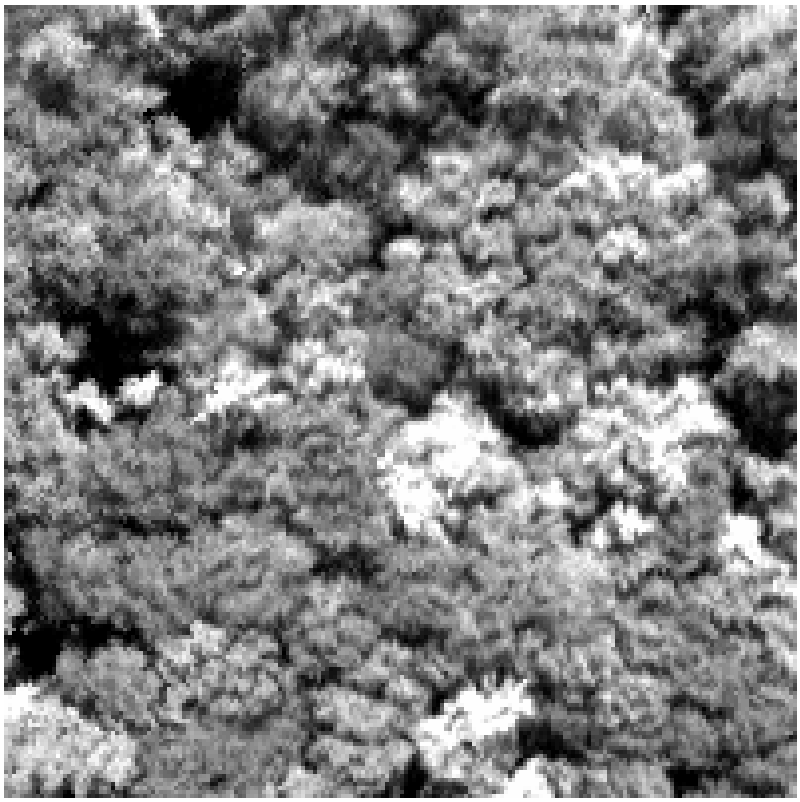


Figure 4.4 Mosaicked and gaussian smoothed green band imagery (550 nm) of the lower study area.

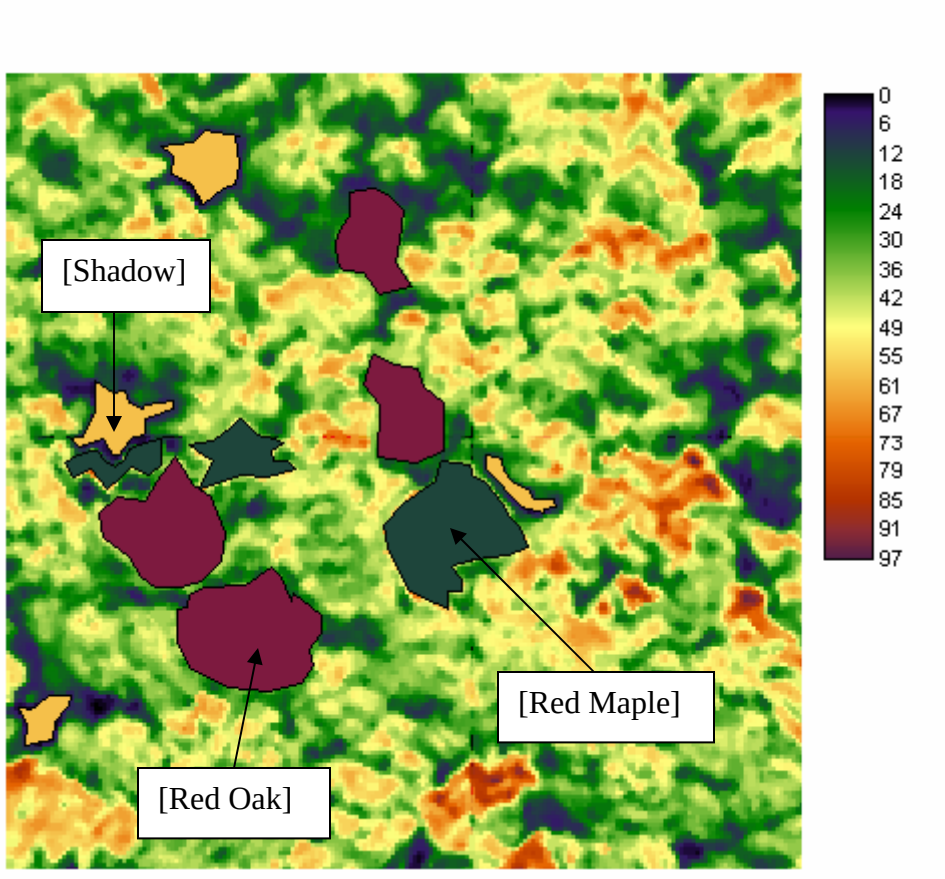


Figure 4.5 False color image demonstrating feature class collection of training data used in image classification.

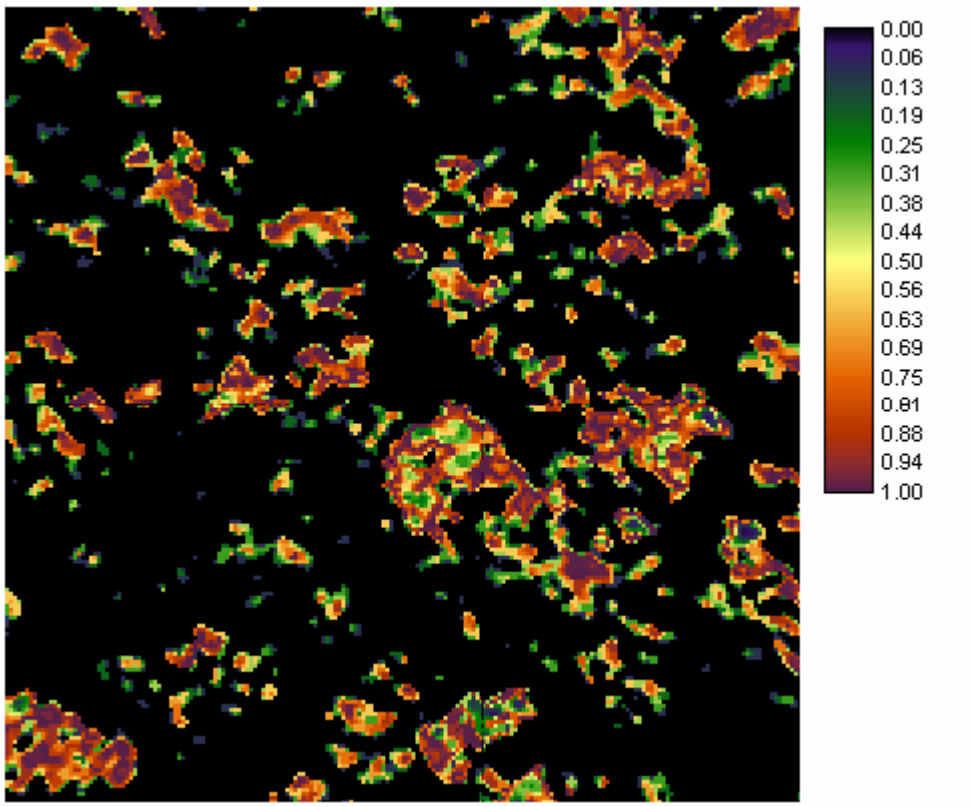


Figure 4.6 Equal probability BELCLASS belief classified surface of [Maple].

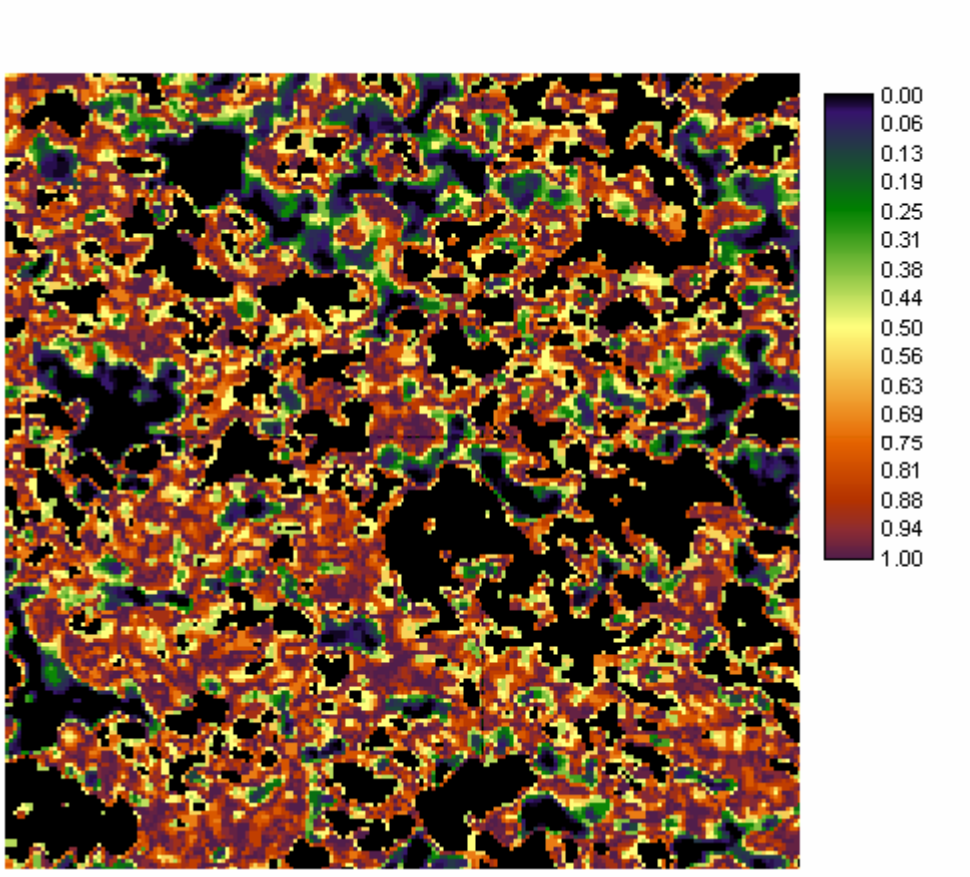


Figure 4.7 Equal probability BELCLASS belief classified surface of [Other] vegetation.

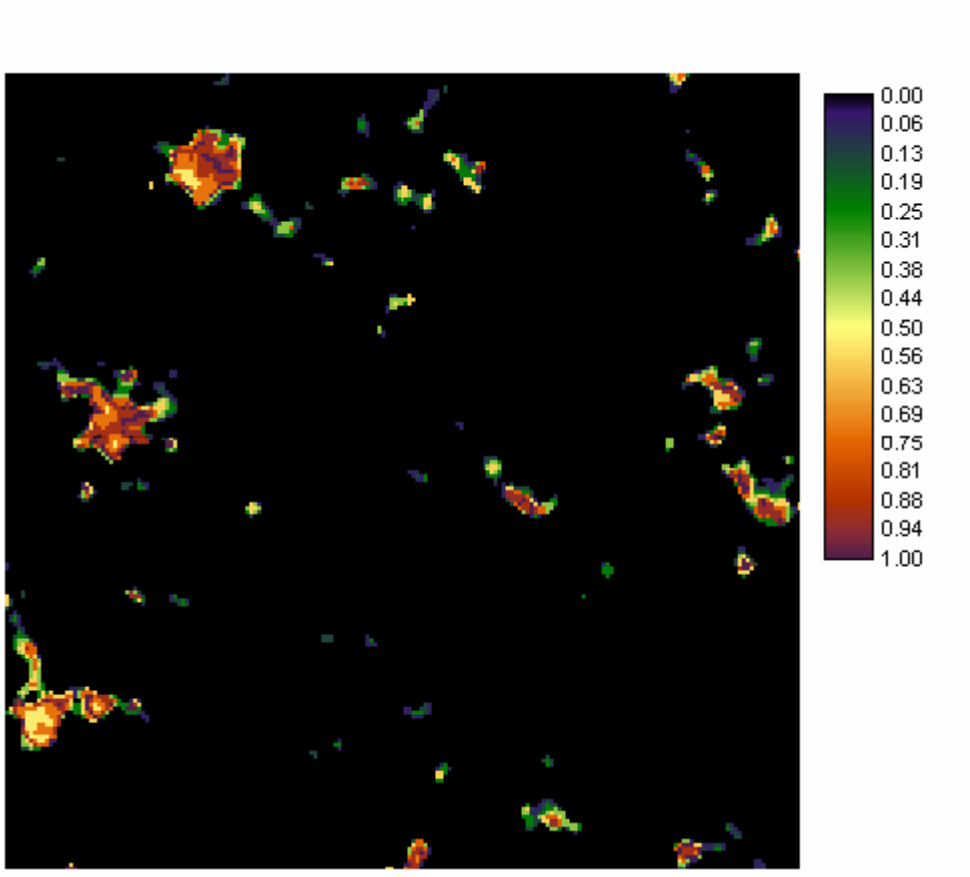


Figure 4.8 Equal probability BELCLASS surface of [Shadow].

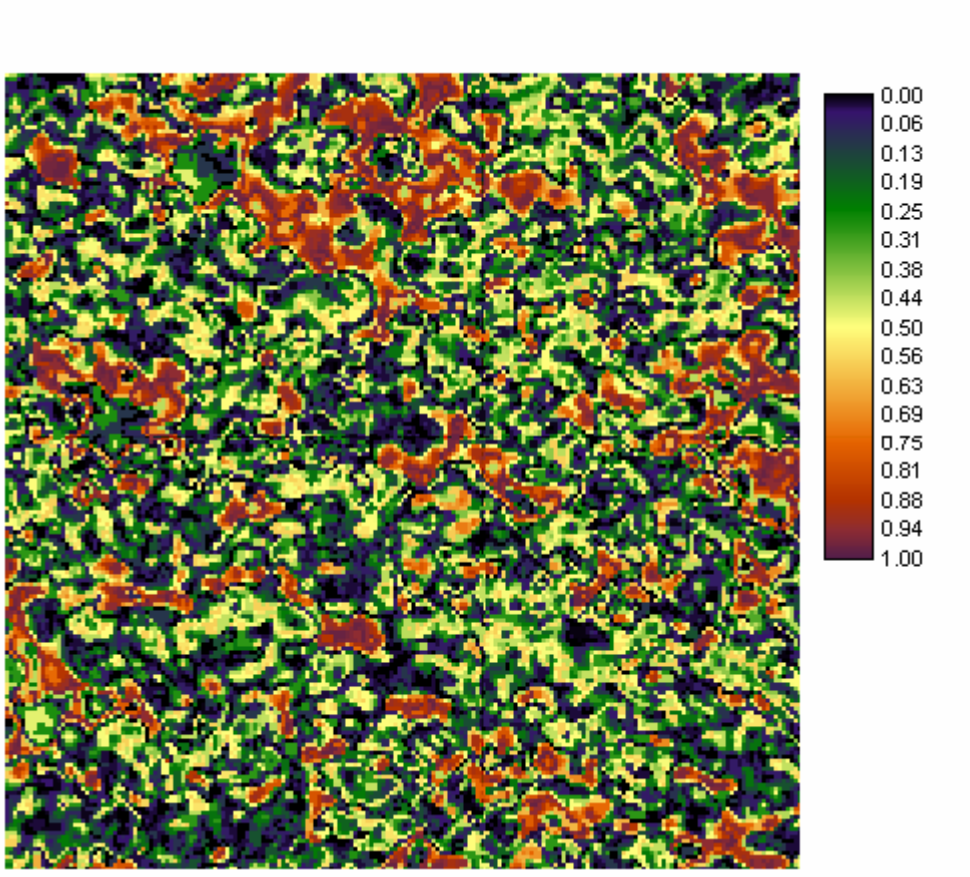


Figure 4.9 Equal probability BELCLASS surface of ignorance expressed as classification uncertainty.

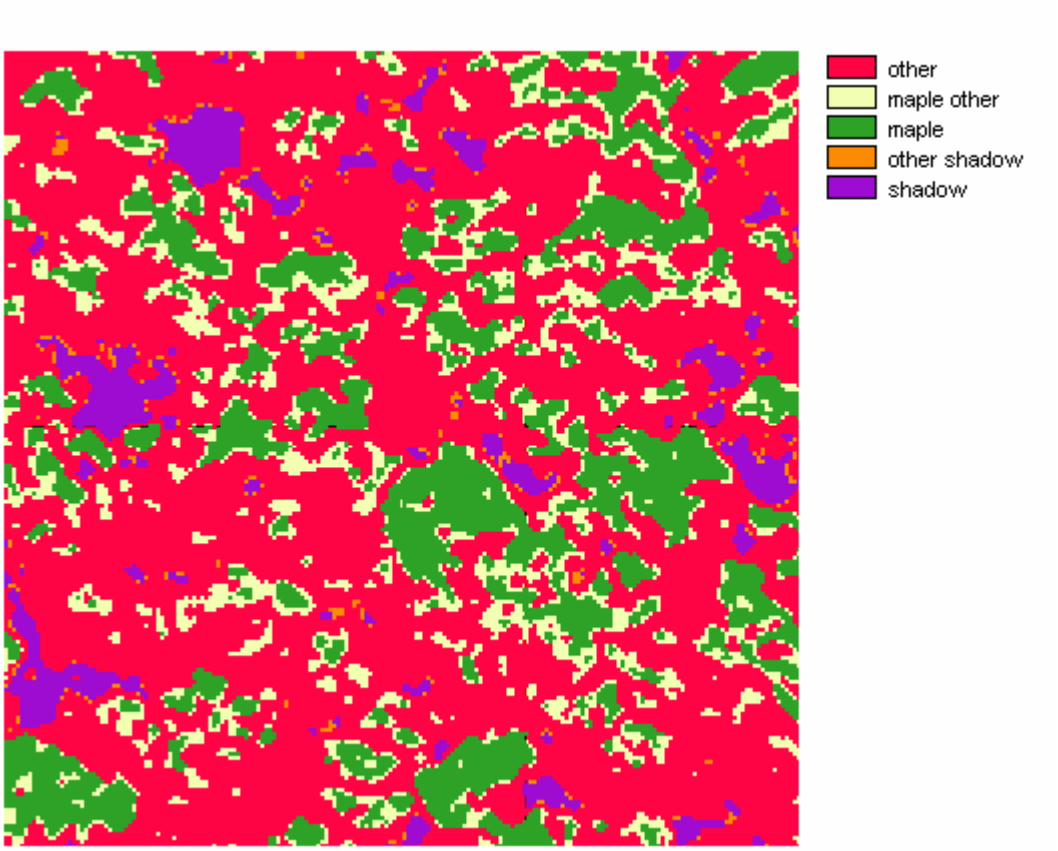


Figure 4.10 Approach 1 results from MAXSET.

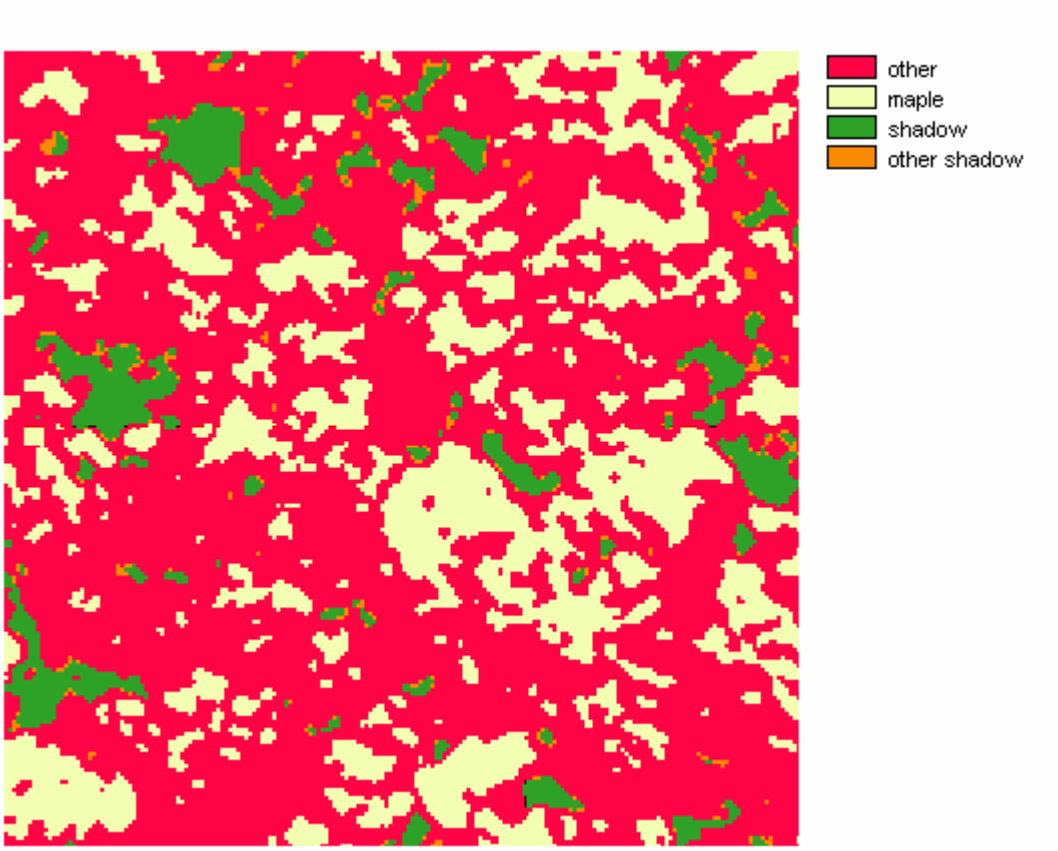


Figure 4.11 Approach 2 results from MAXSET.

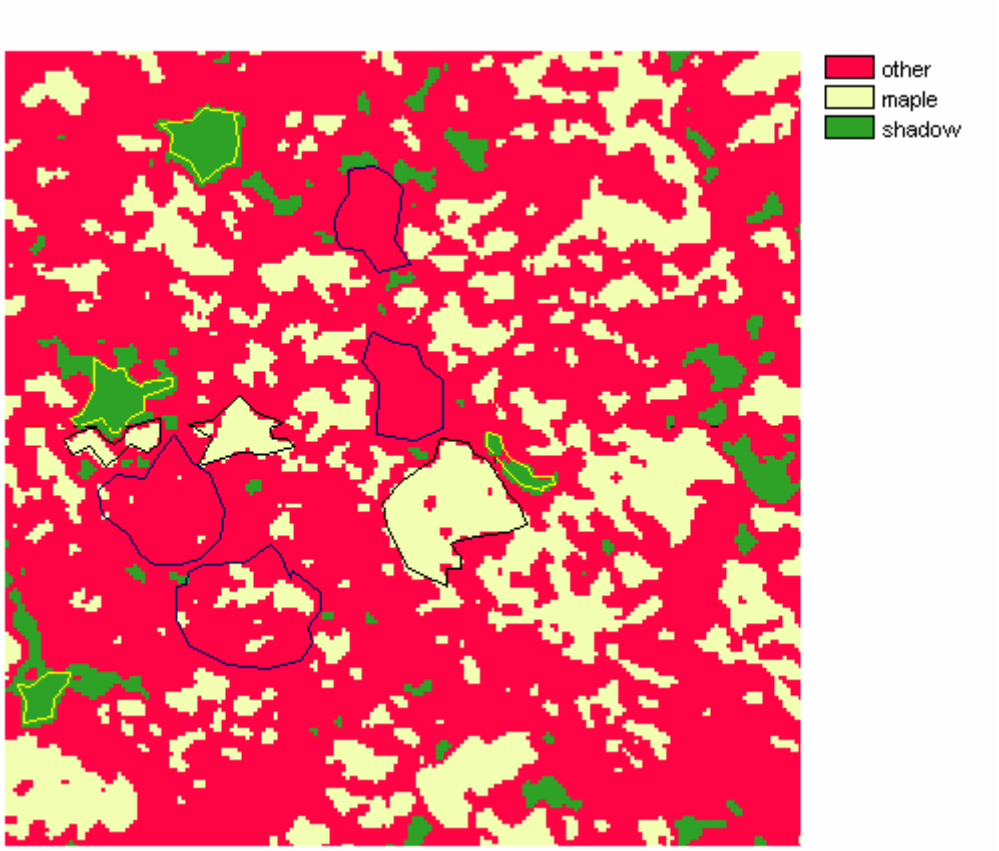


Figure 4.12 Approach 3 results from MAXSET.

References

Aber, J., N. Christensen, I. Fernandez, J. Franklin, L. Hidinger, M. Hunter, J. MacMahon, D. Mladenoff, J. Pastor, D. Perry, R. Slangen, and H. van Miegroet. 2000. Applying ecological principles to management of the U.S. National Forests. Issues in Ecology 6:2-19.

Abrams, M. D. 1998. The red maple paradox: What explains the widespread expansion of red maple in eastern forests? BioScience 48:355-364.

Adams, J. B., Sabol, D.E., Kapos, V., Filho, R.A., Roberts, D.A., Smith, M.O., and A. R. Gillespie. 1995. Classification of multispectral images based on fractions of endmembers: Application to land-cover change in the Brazilian Amazon. Remote Sensing of Environment 52:137-154.

Asner, G. P. 1998. Biophysical and biochemical sources of variability in canopy reflectance. Remote Sensing of Environment 64:234-253.

Asner, G. P., and C.A. Wessman. 1997. Scaling PAR absorption froom the leaf to landscape level in spatially heterogeneous ecosystems. Ecological Modelling 103:81-97.

Asner, G. P., Wessman, C.A., Bateson, C.A., and J.L. Privette. 2000. Impact of tissue, canopy, and landscape factors on the hyperspectral reflectance variability of arid ecosystems. Remote Sensing of Environment 74.

Baret, F., and G. Guyot. 1991. Potentials and limits of vegetation indices for LAI and APAR assessment. Remote Sensing of Environment 35:161-173.

Bastin, L. 1997. Comparison of fuzzy c-means classification, linear mixture modelling, and MLC probabilities as tools for unmixing coarse pixels. International Journal of Remote Sensing 18:3629-3648.

Belward, A. S. 1991. Spectral characteristics of vegetation, soil, and water in the visible, near-infrared, and middle-infrared wavelengths. Pages 31-53 *in* A. S. Belward, Valenzuela, C.R., editor. Remote Sensing and Geographical Information Systems for Research Management in Developing Countries. Kluwer, Dordrecht, Netherlands.

Blackburn, G. A., and E.J. Milton. 1995. Seasonal variation in the spectral reflectance of deciduous tree canopies. International Journal of Remote Sensing 16:709-720.

Boardman, J. W., F.A. Kruse, and R.O. Green. 1995. Mapping target signatures via partial unmixing of AVIRIS data. *In* Summaries, Fifth Annual JPL Airborne Earth Science Workshop, JPL Publication 95-1, v. 1, pp. 23-26.

Bonan, G. B. 1998. The land surface climatology of the NCAR land surface model coupled with the NCAR community climate model. Journal of Climate 11:1307-1327.

Bond, W. J., W. G. Lee, and J. M. Craine. 2004. Plant structural defenses against browsing birds: a legacy of New Zealand's extinct moas. Oikos 104:500-508.

Borel, C. C., and S.A.W. Gerstl. 1994. Nonlinear spectral mixing models for vegetative and soil surfaces. Remote Sensing of Environment 47:403-416.

Bormann, F. H., Siccama, T.G., Likens, G.E., and R.H. Whittaker. 1970. The Hubbard Brook ecosystem study: Composition and dynamics of the tree stratum. Ecological Monographs 40:373-388.

Botkin, D. B., Simpson, L.G., and R.A. Nisbet. 1993. Biomass and carbon storage of the North American deciduous forest. Biogeochemistry 20:1-17.

Boyer, M., Miller, J., Belanger, M., Hare, E., and J. Wu. 1988. Senescence and spectral reflectance of leaves of northern pin oak (*Quercus palustris* Muenchh.). Remote Sensing of Environment 25:71-87.

Brakke, T. W., Wergin, W.P., Erbe, E.F., and J.M. Harnden. 1993. Seasonal variation in the structure and red reflectance of leaves from yellow poplar, red oak, and red maple. Remote Sensing of Environment 43:115-130.

Brandtberg, T., Warner, T.A., Landenberger, R.E., and J.B. McGraw. 2003. Detection and analysis of individual leaf-off tree crowns in small footprint, high sampling density LiDAR data from the eastern deciduous forest in North America. Remote Sensing of Environment 85:290-303.

Campbell, J. B. 1981. Spatial autocorrelation effects upon accuracy of supervised classification of land cover. Photogrammetric Engineering & Remote Sensing 47:355-363.

Caselton, W. F., and W. Luo. 1992. Decision making with imprecise probabilities: Dempster-Shafer theory and application. Water Resources Research 28:3071-3083.

Chason, J. W., D. D. Baldocchi, and M. A. Huston. 1991. A comparison of direct and indirect methods for estimating forest canopy leaf area. Agricultural and Forest Meteorology 57:107-128.

Chen, J. M., Pavlic, G., Brown, L., Cihlar, J., LeBlanc, S.G., White, H.P., Hall, R.J., Peddle, D.R., King, D.J., Trofymow, J.A., Swift, E., Van der Sanden, J., and P.K.E. Pellikka. 2002. Derivation and validation of Canada-wide coarse-resolution leaf area index maps using high-resolution satellite imagery and ground measurements. Remote Sensing of Environment 80:165-184.

Cochrane, M. A. 2000. Using vegetation reflectance variability for species level classification of hyperspectral data. International Journal of Remote Sensing 21:2075-2087.

Congalton, R. G. 1991. A review of assessing the accuracy of classifications of remotely sensed data. Remote Sensing of Environment 37:35-46.

Culvenor, D. S., Coops, N., Preston, R., and K.G. Tolhurst. 1998. A spatial clustering approach to automated tree crown delineation. Pages 67-80 *in* D. A. Hill, Leckie, D.G., editor. Automated Interpretation of High Spatial Resolution Digital Imagery for Forestry, Victoria, British Columbia, Canada.

Dempster, A. P. 1967a. Upper and lower probabilities induced by a multivalued mapping. The Annals of Mathematical Statistics 38:325-339.

Dempster, A. P. 1967b. Upper and lower probability inference based on a sample from a finite univariate population. Biometrika 54:515-528.

Dralle, K.,and M. Rudemo. 1996. Stem number estimation by kernel smoothing of aerial photos. Canadian Journal of Forest Research 26:1228-1236.

Eastman, P. A. K., and E. L. Camm. 1995. Regulation of photosynthesis in interior spruce during water stress: changes in gas exchange and chlorophyll fluorescence. Tree Physiology 15:229-235.

Fassnacht, K. S., Gower, S.T., MacKenzie, M.D., Nordheim, E.V., and T.M. Lillesand. 1997. Estimating the leaf area index of north central Wisconsin forests using the Landsat Thematic Mapper. Remote Sensing of Environment 61:229-245.

Fassnacht, K. S., S.T. Gower, J.M. Norman, and R.E. McMurtie. 1994. A comparison of optical and direct methods for estimating foliage surface area index in forests. Agricultural and Forest Meteorology 71:183-207.

Foody, G. M. 1999. The continuum of classification fuzziness in thematic mapping. Photogrammetric Engineering & Remote Sensing 65:443-451.

Foody, G. M., N. A. Campbell, N. M. Trodd, and T. F. Wood. 1992. Derivation and applications of probabilistic measures of class membership from the Maximum-likelihood classification. Photogrammetric Engineering & Remote Sensing 58:1335-1341.

Foody, G. M., G. Palubinskas, R. M. Lucas, P. J. Curran, and M. Honzak. 1996. Identifying terrestrial carbon sinks: Classification of successional stages in regenerating tropical forest from Landsat TM data. Remote Sensing of Environment 55:205-216.

Foody, G. M., and N. M. Trodd. 1993. Non-classifactory analysis and representation of heathland from remotely sensed imagery. GeoJournal 29:343-350.

Foschi, P., and D. Smith. 1997. Detecting subpixel woody vegetation in digital imagery using two artificial intelligence approaches. Photogrammetric Engineering & Remote Sensing 63:493-500.

Foster, J. R., and P.A. Townsend. 2002. Mapping forest composition in the central Appalachians using AVIRIS: Effects of topography and phenology *in* 2002 AVIRIS Airborne Geoscience Workshop Proceedings. JPL, Pasadena, CA, USA.

Gates, D. M., Keegan, H.J., Schleter, J.C., and V.R. Weidner. 1965. Spectral properties of plants. Applied Optics 4:11-20.

Gausman, H. W. 1985. Plant Leaf Optical Properties in Visible and Near-Infrared Light. Graduate Studies 29, Texas Tech University Press, Lubbock, TX.

Gholz, H. L. 1982. Environmental limits on aboveground net primary production, leaf area, and biomass in vegetation zones of the Pacific Northwest. Ecology 63:469-481.

Glenn, N. F., Mundt, J.T., Weber, K.T., Prather, T.S., Lass, L.W., and J. Pettingill. 2005. Hyperspectral data processing for repeat detection of small infestations of leafy spurge. Remote Sensing of Environment 95:399-412.

Gougeon, F. A. 1997. A locally adaptive technique for forest regeneration assessments from high resolution aerial images. Pages 1-9 *in* 19th Canadian Remote Sensing Symposium. Canadian Aeronautics and Space Institute, Ottawa, Ottawa, Ontario, Canada.

Gower, S. T., Kucharik, C.J., and J.M. Norman. 1999. Direct and indirect estimation of leaf area index, fAPAR, and net primary production of terrestrial ecosystems. Remote Sensing of Environment 70:29-51.

Gower, S. T., Vogt, K.A., and C.C. Grier. 1992. Carbon dynamics of Rocky Mountain Douglas-fir: influence of water and nitrogen availability. Ecological Monographs 62:43-65.

Grier, C. G., and S.W. Running. 1977. Leaf area of mature northwestern coniferous forests: Relation to site water balance. Ecology 58:893-899.

Griffith, D. A. 1987. Spatial Autocorrelation. Association of American Geographers, Washington, D.C.

Hoffer, R. M. 1978. Biological and physical considerations in applying computer aided analysis techniques to remote sensor data. Pages 227-289 *in* P. H. Swain and S. M. Davis, editors. Remote sensing: the quantitative approach. McGraw Hill, New York.

Hoover, C. M., Birdsey, R.A., Heath, L.S., and S.L. Stout. 2000. How to estimate carbon on small forest tracts. Journal of Forestry September:13-19.

Howard, J. A. 1991. Remote Sensing of Forest Resources: Theory and application. Chapman & Hall, Cambridge.

Jacquemoud, S., Baret, F., Andrieu, B., Danson, F.M., and K. Jaggard. 1995. Extraction of vegetation biophysical parameters by inversion of the PROSPECT + SAIL models on sugar beet canopy reflectance data. Application to TM and AVIRIS sensors. Remote Sensing of Environment 52:163-172.

Jahne, B. 1991. Digital Image Processing. Pages 219-230 *in*. Springer-Verlag, New York.

Jain, A. K. 1989. Fundamentals of Digital Image Processing. *in*. Prentice Hall, Englewood Cliffs, NJ.

Jensen, J. R. 1983. Biophysical Remote Sensing. Annals of the Association of American Geographers 73:111-132.

Jin, M., and D..-L. Zhang. 2002. Observed variations of leaf area index and its relationship with surface temperatures during warm seasons. Meteorology and Atmospheric Physics 80:117-129.

Jordan, C. F. 1969. Derivation of leaf-area index from quality of light on the forest floor. Ecology 50:663-666.

Jurik, T. W., G.M. Briggs, and D.M. Gates. 1985. A comparison of four methods for determining leaf area index in successional hardwood forests. Canadian Journal of Forest Research 15:1154-1158.

Kergoat, L. 1998. A model for hydrological equilibrium of leaf area index on a global scale. Journal of Hydrology 212-213:268-286.

Key, T., Warner, T.A., McGraw, J., and M.A. Fajvan. 1998. An evaluation of the relative value of spectral and phenological information for tree crown classification of digital images in the eastern deciduous forest. Pages 243-254 *in* D. A. Hill, Leckie, D.G., editor. Automated Interpretation of High Spatial Resolution Digital Imagery for Forestry. Natural Resources Canada, Canadian Forest Service, Pacific Forestry Centre, Victoria, British Columbia, Canada.

Key, T., Warner, T.A., McGraw, J.B., and M.A. Fajvan. 2001. A comparison of multispectral information in high spatial resolution imagery for classification of individual tree species in a temperate hardwood forest. Remote Sensing of Environment. 75:100-112.

Knipling, E. B. 1970. Physical and physiological basis for the reflectance of visible and near-infrared radiation from vegetation. Remote Sensing of Environment 1:155-159.

Kriegler, F. J., W. A. Malila, R. F. Nalepka, and W. Richardson. 1969. Preprocessing transformations and their effects on multispectral recognition. Pages 97-131 *in* Sixth International Symposium on Remote Sensing of Environment. University of Michigan, Ann Arbor, MI.

Larcher, W. 1995. Physiological plant ecology: ecophysiology and stress physiology of functional groups, 3rd edition. Springer-Verlag, New York.

Le Hegerat-Mascle, S., I. Bloch, and D. Vidal-Madjar. 1997. Application of Dempster Shafer Evidence Theory to unsupervised classification in multisource remote sensing. IEEE Transactions on Geoscience and Remote Sensing 35:1018-1031.

Le Hegerat-Mascle, S., A. Quesney, D. Vidal-Madjar, O. Taconet, M. Normand, and C. Loumagne. 2000. Land cover discrimination from multitemporal ERS images and multispectral Landsat images: a study case in an agricultural area in France. International Journal of Remote Sensing 21:435-456.

Leckie, D. G., Gillis, M.D., Gougeon, F., Lodin, M., Wakelin, J., and X. Yuan. 1998. Computer-assisted photointerpretation aids to forest inventory mapping: Some possible approaches. Pages 205-213 *in* Fourth International Airborne Remote Sensing Conference and Exhibition/21st Canadian Symposium on Remote Sensing. ERIM International Inc., Ann Arbor, MI, USA, Ottawa, Canada.

Leckie, D. G., Smith, N., Davison, D., Jay, C., Gougeon, F., Achal, S., Burnett, C., Cloney, E., Lataille, S., Montgomery, F., Nelson, T., and N. Walsworth. 1999. Automated interpretation of high spatial resolution multispectral (CASI) imagery: A development project for a forestry company. Pages 201-211 *in* Fourth International Airborne Remote Sensing Conference and Exhibition/21st Canadian Symposium on Remote Sensing. ERIM International Inc., Ann Arbor, MI, USA, Ottawa, Canada.

Leckie, D. G., Yuan, X., Ostaff, D.P., Piene, H., and D.A. MacLean. 1992. Analysis of high resolution multispectral MEIS imagery for spruce budworm damage assessment on a single tree basis. Remote Sensing of Environment 40:125-136.

Lein, J. K. 2003a. Applying evidential reasoning methods to agricultural land cover classification. International Journal of Remote Sensing 24:1-20.

Lein, J. K. 2003b. Sensing sprawl: Towards the monitoring of urban expansion using Dempster-Shafer theory. Geocarto International 18:61-70.

Likens, G. E. 1999. The science of nature, the nature of science: Long-term ecological studies at Hubbard Brook. Proceedings of the American Philosophical Society 143:558-572.

Liu, J., Chen, J.M., Cihlar, J., and W.M. Park. 1997. A process-based boreal ecosystem productivity simulator using remote sensing inputs. Remote Sensing of Environment 62:158-175.

Lorimer, C. G. 1984. Development of the red maple understory in northeastern oak forests. Forest Science 30:3-22.

MacQueen, J. B. 1967. Some Methods for classification and Analysis of Multivariate Observations. Pages 281-297 *in* 5th Berkeley Symposium on Mathematical Statistics and Probability. University of California Press, Berkeley.

Martin, M. E., and J.D. Aber. 1997. High spectral resolution remote sensing of forest canopy lignin, nitrogen, and ecosystem processes. Ecological Applications 7:431-443.

Martin, M. E., Newman, S.D., Aber, J.D., and R.G. Congalton. 1998. Determining forest species composition using high spectral resolution remote sensing data. Remote Sensing of Environment 65:249-254.

Mazer, A. S., M. Martin, M. Lee, and J. E. Solomon. 1988. Image Processing Software for Imaging Spectrometry Analysis. Remote Sensing of Environment 24:201-210.

McLellan, T. M., J. D. Aber, M. E. Martin, J. M. Melillo, and K. J. Nadelhoffer. 1991. Determination of nitrogen, lignin and cellulose content of decomposing leaf material by near infrared reflectance spectroscopy. Canadian Journal of Forest Research 21:1684-1688.

Motzkin, G., P. Wilson, D. R. Foster, and A. Allen. 1999. Vegetation patterns in heterogeneous landscapes: The importance of history and Environment. Journal of Vegetation Science 10:903-920.

Muchoney, D. M., and A. H. Strahler. 2002. Pixel- and site-based calibration and validation methods for evaluating supervised classification of remotely sensed data. Remote Sensing of Environment 81:290-299.

Myneni, R. B., Hall, F.G., Sellers, P.J., and A.L. Marshak. 1995. The interpretation of spectral vegetation indices. IEEE Transactions On Geoscience and Remote Sensing 33:481-486.

Myneni, R. B., Hoffman, S., Knyazikhin, Privette, J.L., Glassy, J., Tian, Y., Wang, Y., Song, X., Zhang, Y., Smith, G.R., Lotsch, A., Freidl, M., Morisette, J.T., Votava, P., Nemani, R.R., and S.W. Running. 2002. Global products of vegetation leaf area and fraction absorbed PAR from year one of MODIS data. Remote Sensing of Environment 83:214-231.

Myneni, R. B., Ross, J., and G. Asrar. 1989. A review on the theory of photon transport in leaf canopies. Agricultural and Forest Meteorology 45:1-15.

Nemani, R., Pierce, L., and S. Running. 1993. Forest ecosystem processes at the watershed scale: sensitivity to remotely-sensed Leaf Area Index estimates. International Journal of Remote Sensing 14:2519-2534.

Neumann, H. H., Hartog, G., and R.H. Shaw. 1989. Leaf area measurements based on hemispheric photographs and leaf-litter collection in a deciduous forest during autumn leaf-fall. Agricultural and Forest Meteorology 45:325-345.

Pouliot, D. A., King, D.J., Bell, F.W., and D.G. Pitt. 2002. Automated tree crown detection and delineation in high-resolution digital camera imagery of coniferous forest regeneration. Remote Sensing of Environment:322-334.

Price, J. C. 1992. Variability of high-resolution crop reflectance spectra. International Journal of Remote Sensing 13:2593-2610.

Price, J. C. 1994. How unique are spectral signatures? Remote Sensing of Environment 49:181-186.

Price, J. C., and W.C. Bausch. 1995. Leaf area index estimation from visible and near-infrared reflectance data. Remote Sensing of Environment 52:55-65.

Ramsey III, E., Rangoonwala, A., Nelson, G., and Ehrlich, R. 2005a. Mapping the invasive species, Chinese tallow, with EO1 satellite Hyperion hyperspectral image data and relating tallow occurrences to a classified Landsat Thematic Mapper land cover map. International Journal of Remote Sensing 26:1637-1657.

Ramsey III, E., Rangoonwala A., Nelson, G., Ehrlich, R, and Martella, K. 2005b. Generation and validation of characteristic spectra from EO1 Hyperion image data for detecting the occurence of the invasive species, Chinese tallow. International Journal of Remote Sensing 26:1611-1636.

Reicosky, D. C. 1994. Diurnal trends in wheat canopy temperature, photosynthesis, and evapotranspiration. Remote Sensing of Environment 49:235-245.

Richards, J. A. 1993. Remote Sensing Digital Image Analysis. Springer-Verlag, New York.

Roberts, D. A., Adams, J.B., and M.O. Smith, M.O. 1993. Green vegetation, nonphotosynthetic vegetation, and soil in AVIRIS data. Remote Sensing of Environment 14:255-269.

Roberts, D. A., Nelson, B.W., Adams, J.B., and F. Palmer. 1998. Spectral changes with leaf aging in Amazon *caatinga*. Trees 12:315-325.

Roberts, D. A., SMith, M.O., Adams, J.B., Sabol, D.E., Gillespie, A.R., and S.C. Willis. 1990. Isolating woody plant material and senescent vegetation from green vegetation in AVIRIS data. Pages 42-57 *in* R.O. Green, editor. 2nd Airborne Visible/Infrared Imaging Spectrometer (AVIRIS) Workshop. JPL, Pasadena, CA.

Rohde, W. G., Olson, C.E.Jr. 1972. Multispectral sensing of forest tree species. Photogrammetric Engineering:1209-1215.

Ross, J. 1981. The Radiation Regime and Architecture of Plant Stands. Junk, The Hague.

Rouse, J. W., Haas, R,H., Deering, D.W., and J.A. Schell. 1974. Monitoring the vernal advancement and retrogradation (Green wave effect) of natural vegetation. Final Report RSC 1978-4. Remote Sensing Center, Texas A&M University, College Station, TX.

Sanger, J. E. 1971. Quantitative investigation of leaf pigments from their inception in buds through autumn coloration to decomposition in falling leaves. Ecology 52:1075-1089.

Sellers, P. J., R. E. Dickinson, D. A. Randall, A. K. Betts, F. G. Hall, J. A. Berry, G. J. Collatz, A. S. Denning, H. A. Mooney, C. A. Nobre, N. Sato, C. B. Field, and A. Henderson-Sellers. 1997. Modeling the exchanges of energy, water, and carbon between continents and the atmosphere. Science 275:502-508.

Settle, J. J., and N. A. Drake. 1993. Linear mixing and the estimation of ground cover proportions. International Journal of Remote Sensing 14:1159-1177.

Shafer, S. L., P. J. Bartlein, and R. S. Thompson. 2001. Potential Changes in the Distributions of Western North America Tree and Shrub Taxa under Future Climate Scenarios. Ecosystems 4:200-215.

Sinclair, T. R., Hoffer, R.M., and M.M. Schreiber. 1971. Reflectance and internal structure of leaves from several crops during a growing season. Agronomy Journal 63:864-867.

Slaton, M. R., Hunt, E.R. Jr., and W.K. Smith. 2001. Estimating near-infrared leaf reflectance from leaf structural characteristics. American Journal of Botany 88:278-284.

Smith, T. M., H. H. Shugart, and F. I. Woodward. 1997. Plant Functional Types: Their Relevance to Ecosystem Properties and Global Change. Cambridge University Press, Cambridge.

Sohn, Y., and R. M. McCoy. 1997. Mapping desert shrub rangeland using spectral unmixing and modeling spectral mixtures with TM data. Photogrammetric Engineering & Remote Sensing 63:707-716.

Thomas, J. R., Wiegand, C.L., and V.I. Myers. 1967. Reflectance of cotton leaves and its relation to yield. Agronomy Journal 59:551-554.

Tift, B. D., and M. A. Fajvan. 1999. Red maple dynamics in Appalachian hardwood stands in West Virginia. Canadian Journal of Forest Research-Revue Canadienne De Recherche Forestiere 29:157-165.

Turnbull, M. H., Whitehead, D., Tissue, D.T., Schuster, W.S.F., Brown, K.J., Engel, V.C., and K.L. Griffin. 2002. Photosynthetic characteristics in canopies of *Quercus rubra*, *Quercus prinus*, and *Acer rubrum* differ in response to soil water availability. Oecologia 130:515-524.

Tyron, H. H. 1930. The Black Rock Forest Bulletin No. 1. The Black Rock Forest, Cornwall-On-The-Hudson, New York.

van Aardt, J.A.N., and R.H. Wynne. 2001. Spectral separability among six southern tree species. Photogrammetric Engineering & Remote Sensing 67:1367-1375.

Waring, R. H., Law, B.E., Goulden, M.L., Bassow, S.L., McCreight, R.W., Wofsy, S.C., and F.A. Bazzaz. 1995. Scaling gross ecosystem production at Harvard Forest with remote sensing: a comparison of estimates from a constrained quantum-use efficiency model and eddy correlation. Plant, Cell, and Environment 18:1201-1213.

Waring, W., and W. Schlesinger. 1985. Forest Ecosystems: Concepts and Management. Academic Press, Inc., Toronto, Ontario, Canada.

Warner, T., McGraw, J., Dean, C., and R. Landenberger. 2000. Automatic delineation of individual deciduous trees in high resolution imagery. Pages 144-147 *in* The 28th International Symposium on Remote Sensing of Environment, Cape Town, South Africa.

Warner, T. A., Lee, J.L., and J.B. McGraw. 1998. Delineation and identification of individual forest trees in the eastern deciduous forest. Pages 81-91 *in* D.A. Hill, Leckie, D.G., editors. Automated Interpretation of High Spatial Resolution Digital Imagery for Forestry, Victoria, British Columbia, Canada.

Watson, D. J. 1947. Comparative physiological studies on the growth of field crops. Annals of Botany 11:1947.

Weiss, M., F. Baret, G. J. Smith, I. Jonckheere, and P. Coppin. 2004. Review of methods for *in situ* leaf area index (LAI) determination Part II. Estimation of LAI, errors and sampling. Agricultural and Forest Meteorology 121:37-53.

Whitmore, T. C., N. D. Brown, M. D. Swaine, D. Kennedy, C. I. Goodwin-Bailey, and W.-K. Gong. 1993. Use of hemispherical photographs in forest ecology: Measurement of gap size and radiation totals in a Bornean tropical rain forest. Journal of Tropical Ecology 9: 131-151.

Whittaker, R. H., Bormann, F.H., Likens, G.E., and T.G. Siccama. 1974. The Hubbard Brook ecosystem study: Forest biomass and production. Ecological Monographs 44:233-254.

Williams, D. L. 1991. A comparison of spectral reflectance properties at the needle, branch, and canopy level for selected conifer species. Remote Sensing of Environment 35:79-93.

Williams, M. 1996. Modelling the soil-plant-atmosphere continuum in a *Quercus-Acer* stand at Harvard Forest: the regulation of stomatal conductance by light, nitrogen and soil/plant hydraulic properties. Plant, Cell and Environment 19:911-927.

Woolley, J. T. 1971. Reflectance and transmittance of light by leaves. Plant Physiology 47:656-662.

Wulder, M., Niemann, K.O., and D.G. Goodenough. 2000. Local maximum filtering for the extraction of tree locations and basal area from high spatial resolution imagery. Remote Sensing of Environment 73:103-114.

Zadeh, L. A. 1965. Fuzzy sets. IEEE Transactions Information and Control 8:338-353.

Zadeh, L. A. 1973. Outline of a new approach to the analysis of complex systems and decision processes. IEEE Transactions on Systems, Man and Cybernetics SMC-3:28-44.